

# Lawrence Berkeley National Laboratory

## Recent Work

### **Title**

MATERIALS SCIENCE OF MODERN STEELS

### **Permalink**

<https://escholarship.org/uc/item/4783s835>

### **Authors**

Parker, Earl R.  
Zackay, Victor F.

### **Publication Date**

1973-10-01

To be published as a chapter in  
"Solid State Chemistry", Volume 9,  
Pergamon Press

LBL-2286  
Preprint *c.2*

MATERIALS SCIENCE OF MODERN STEELS

Earl R. Parker and Victor F. Zackay

October 1973

**RECEIVED**  
LAWRENCE  
RADIATION LABORATORY

JAN 22 1974

AEC Contract No. W-7405-ENG-48

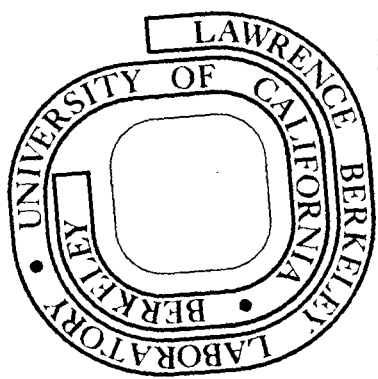
**LIBRARY AND  
DOCUMENTS SECTION**

and

AMMRC Contract No. DAAG46-73-C-0120

**TWO-WEEK LOAN COPY**

*This is a Library Circulating Copy  
which may be borrowed for two weeks.  
For a personal retention copy, call  
Tech. Info. Division, Ext. 5545*



LBL-2286  
*c.2*

## **DISCLAIMER**

This document was prepared as an account of work sponsored by the United States Government. While this document is believed to contain correct information, neither the United States Government nor any agency thereof, nor the Regents of the University of California, nor any of their employees, makes any warranty, express or implied, or assumes any legal responsibility for the accuracy, completeness, or usefulness of any information, apparatus, product, or process disclosed, or represents that its use would not infringe privately owned rights. Reference herein to any specific commercial product, process, or service by its trade name, trademark, manufacturer, or otherwise, does not necessarily constitute or imply its endorsement, recommendation, or favoring by the United States Government or any agency thereof, or the Regents of the University of California. The views and opinions of authors expressed herein do not necessarily state or reflect those of the United States Government or any agency thereof or the Regents of the University of California.

MATERIALS SCIENCE OF MODERN STEELS

Earl R. Parker and Victor F. Zackay

Center for the Design of Alloys  
Inorganic Materials Research Division, Lawrence Berkeley Laboratory and  
Department of Materials Science and Engineering, College of Engineering;  
University of California, Berkeley, California 94720

ABSTRACT

The evolution of steelmaking technology is traced from its primitive origins nearly four thousand years ago to its present highly sophisticated forms. The emergence of physical metallurgy is shown to be largely associated with the burst of activity in the physical sciences in the last one hundred years. The suggestion is made that a new era in physical metallurgy has now begun, viz, the era of alloy design, which is characterized by the application of the first principles of materials science to the creation of new and superior engineering alloys. It is postulated that this new era could not have started without a preceding one in which the analytical and experimental tools (pre-requisite for an atomistic understanding of solids) were brought to high levels of sophistication. The current status of alloy design is represented by several illustrative examples taken from current research. The "design" of these alloys is shown to consist of a mixture of science, engineering and empiricism. The remaining but ever-diminishing component of empiricism is considered to be one of the existing challenges in the continuing story of the technology of steel.



MATERIALS SCIENCE OF MODERN STEELS

Earl R. Parker and Victor F. Zackay

INTRODUCTION

There is a scientific revolution in progress in one of the oldest arts practised by modern man--the making and treating of steel. For 3000 years, civilized men have known how to produce steel--an alloy of iron and carbon. Steel comprises ninety percent of all of the metallic materials in use today. Because of its widespread importance, steel has been the subject of intensive investigations over a long period of time, first by the early users who needed strong tough steel for weapons, then by the entrepreneurs of the last century whose industrial empires depended upon steel for rapid growth, and finally in modern times by researchers searching for safer materials to meet advanced technological requirements. The extensive investigations on the nature of reactions that occur in solid steels have yielded bountiful results. The storehouse of knowledge in this area has increased enormously in the past several decades. This has led many people to believe that continued financial support for basic research in this area is not necessary. As a consequence, a number of large companies, formerly major supporters of large materials science research groups, have either entirely eliminated their efforts in this area, or greatly reduced them. Surprisingly, the valuable knowledge accumulated over a quarter of a century has remained virtually unused. In spite of the existence of this knowledge, no new steels have appeared on the market. Every steel used today is the product of an accidental discovery made 20 to 50 years ago. Only a handful of

people realize that the available basic understanding of the complex reactions that occur in solid steels can now be put to use to design new alloys having properties superior to those of the commercially available materials.

The purpose of this paper is to describe some of the concepts of materials science and to show how the use of these concepts can lead to the discovery of new alloys. Before entering this discussion, however, it will be helpful to obtain a perspective of the historical nature of the subject, starting with the remarkable discoveries by ancient civilizations of how steel could be made and heat treated to enhance its properties, through the scientific investigations of the first half of this century that provided the insight required for understanding the mechanical properties of metals, to the remarkable advances of recent times which have permitted researchers to peer inward to the extent that they could actually observe the behavior of individual atoms in metallic crystals.

#### EARLY HISTORY

Seven metals were used by ancient civilizations. The first two of these, gold and copper, are found in the metallic state in nature. They were used before the year 5000 B.C. Silver, which is also found in small quantities in the native state, came into use almost as early as gold and copper. However, the amount of silver available at that time was much less than the amounts of gold and copper. Lead, the oxide of which is easily reduced by charcoal, was first discovered in the ashes of camp

fires and was used prior to 2500 B.C. The oldest known piece of elementary tin cannot be dated earlier than about 1500 B.C., although bronzes, which are alloys of copper and tin, were available long before that date. Tin is never found in the elementary state but ores consisting of mixtures of tin oxide and copper oxide are quite widespread, and alloys produced from these mixed ores were the source of the bronzes of ancient people. The last of the seven metals used in antiquity were iron and mercury. Iron was rather extensively used because of its high strength and desirable properties, whereas mercury received little attention because of its limited utility.

After about 1200 B.C., iron-making was conducted on a small scale in a number of places in Africa, Asia and Europe. Ores suitable for smelting appeared as outcrops in many areas. In Syria the production of iron became a substantial industry before the end of the second millennium B.C. In Asia Minor activity reached its peak about 1800 B.C., and the Persians began making iron about 1100 B.C. By the year 700 B.C., large quantities of iron were produced and used for tools and weapons. In one archeological discovery, 160 tons of iron in the form of bars suitable for forging into weapons, along with iron chain and other items, was discovered among the remains found in an ancient storehouse. The method for producing iron objects in antiquity differed significantly from the production of objects made of the other seven known metals. This was because the melting point of iron is very high and it was not possible to obtain temperatures high enough to melt steel until about 1740 A.D. Consequently, the ancient smiths were compelled to fashion their products by hammering and welding

pieces of iron together in the solid state. In order to convert iron to steel, it is necessary to introduce small amounts of carbon. The ancient people could not melt iron and consequently they had to introduce carbon into solid iron. This was probably the first practical use of a solid state diffusion process. The method they used to carburize iron was to heat the metal for a long time in contact with a carbonaceous material such as hot charcoal. Another remarkable discovery of the ancients was the process of hardening steel by quenching it from a red heat into water. This invention was made around 900 B.C. Hardened steel tools made around 800 B.C. have been found in both Assyria and Egypt. Beginning about 600 B.C., iron making was actively pursued in the Noric Alps region. However, the art was not practised in other parts of Europe until Roman times, except in a small way in local regions. By 400 B.C. the Celts were the principal makers of iron and were primarily responsible for the spread of iron working before the Roman period. The heat treating of steel was practised widely by the Romans, but the control of quality was relatively poor. They had no accurate means for measuring elevated temperatures and it was therefore difficult to control carburization and hardening processes. The Romans also developed to a high degree the art of joining metals. This was necessary because iron, which could only be made in relatively small pieces, had to be joined by hammer welding to produce large objects. They also developed solders and brazing compounds for the purpose of joining pieces of iron. Little progress was made in metallurgy during the thousand year period following the Roman Empire. During the dark ages the uses of iron and steel did not change significantly, weapons remaining the main product line.

The early ideas about metals and the processes for producing them prevailed until about 1700 A.D. It was at this time that a complete revolution in the modes of philosophical and scientific thinking occurred. In the seventeenth century coal replaced charcoal in the smelting of iron. This permitted, along with changes in furnace design, the attainment of higher temperatures which in turn permitted iron-carbon alloys to be melted and cast into molds. There is a low melting iron-carbon eutectic which contains about 4 pct of carbon. This is much higher than the carbon content of steels, and the resulting product, called cast iron, is brittle. This cast iron was converted into wrought iron by oxidizing the carbon to remove it from the metal. The design of furnaces had been improved to the extent that in 1700 furnaces could produce 2½ tons of cast iron per day. The gaseous products from coal caused considerable trouble in the making of iron and steel, and by the middle of the 18th century, coke began to replace coal as the fuel used in the reduction of iron. The rate of metallurgical developments abated after about 1790 and the methods of production and fabrication used until about 1850 differed little from those employed prior to 1800.

The need for temperatures high enough to melt steel, above 1500°C, became apparent in the mid-19th century. This was eventually accomplished by preheating the air going into the furnace. The major breakthrough in steel production, which introduced the modern technological method for producing steel in extremely large quantities, was invented by Henry Bessemer in 1856. He conceived the idea of blowing air into molten pig iron to raise the temperature of the metal to such heights that the metal was completely decarburized and heated to a sufficiently high temperature

to produce a very fluid metal. The result of the Bessemer process was that the metal could be cast as steel, and therefore could be forged or formed into useful shapes in contrast to cast iron which, because of its extreme brittleness, could not be deformed after casting. Bessemer's first commercial furnace was in operation in 1859. However, the process excessively oxidized the metal leading to a steel with high oxygen contents. Bessemer overcame the disadvantage by adding manganese which reduced the oxygen content of the steel, thus making it more usable. The Bessemer process had one serious disadvantage which could not be overcome by adding corrective elements. This was the absorption of nitrogen by iron when air was blown through the molten metal. Nitrogen in steel has the deleterious effect of making steel behave in a brittle manner under certain conditions. This objectionable effect was quickly discovered. Its solution lay in the design of a completely different kind of furnace for making steel, one that was invented by William Siemens in the 1860's. Siemens designed what is called an open-hearth furnace in which gas, burned with highly preheated air, is passed from one end to the other of the hearth over a relatively thin, flat layer of molten steel. The open-hearth furnace is still widely used. The advantage of the open-hearth method over the Bessemer process is that much larger quantities of metal can be handled in a single charge and there is little nitrogen absorption by the metal. The open-hearth furnaces grew in size as the years went by, reaching capacities of well over 200 tons of molten steel. The open-hearth furnace was used for making practically all steels until very recent times. The Bessemer process is much faster, and consequently more economical to use than the open-hearth method, but its use depended upon

obtaining nitrogen-free oxygen at a low enough price to make the Bessemer-type process economically competitive with the open-hearth furnace. Technological improvements in gas separation processes finally made this possible. During the last ten years there has been a major trend away from the use of open-hearth furnaces back to what is now called the BOF process (basic-oxygen-furnace). This modern revision of the Bessemer process produces a superior grade of steel at a faster rate than any other process available today.

The need for steels having properties superior to those containing only iron and carbon as the major elements became evident around 1900. The addition of other elements to steel, such as nickel and chromium, began to be explored in the early part of the present century. The next section will deal with the development of alloy steels and the need that subsequently arose for an understanding of the nature of the internal structure of the solid steels, and the relation of that structure to the technologically useful properties of the material.

#### MODERN PHYSICAL METALLURGY

Curiosity about the internal structure and nature of iron dates back many centuries. The fact that iron loses its ferromagnetism when heated red hot was discovered in 1600, and before 1800 the idea that iron exhibited an allotropic transformation was proposed. By 1873 the evidence for the transformation had been experimentally provided by measurements of the sudden length change that occurs when the crystal structure changes on heating from body centered cubic to face centered cubic at the critical

temperature. Simultaneously, the thermoelectromotive force was observed to change abruptly. Positive proof of the change in crystal structure was eventually provided by X-ray diffraction evidence, but not until after the turn of the century.

Quantitative measurements of the mechanical properties of metals received increasing attention near the end of the nineteenth century. Earlier landmarks in the history of quantitative mechanics of materials were the discovery of the linear elastic behavior of metals by Hooke in 1660, and the formulation of the general equations of elasticity by Navier in 1821. However, the nature of the variations in internal structure that were responsible for differences in the mechanical properties of a given steel remained obscure until recent times.

The study of the internal structure of metals and alloys, called metallography was an outgrowth of the work of mineralogists and crystallographers in the early nineteenth century. The crystals in metals, however, are unlike most of those in minerals in that they are generally much too small to be observed by eye. Consequently, it was not until methods for microscopic examination were devised that it became possible to study in detail the internal changes in steels produced by alloying, heat treating, and deforming mechanically. Henry C. Sorby of Sheffield, who founded the science of petrography in 1849, was the first to publish major papers on the metallography of steel (1886 and 1887)<sup>1,2</sup> Using magnifications up to 650 times, Sorby identified crystals of iron intermixed with a "pearly constituent" (now called pearlite) consisting of alternate plates of iron and an extremely hard iron-carbon compound (now



known to be  $\text{Fe}_3\text{C}$ ). He also observed that steel hardened by quenching from a high temperature did not contain carbide particles, but that reheating to an intermediate temperature caused carbide particles to form in the steel. In his second paper, Sorby reported the occurrence of recrystallization, the process whereby new small crystals in deformed metal form when the metal is heated. He commented lucidly about the state of "unstable equilibrium" produced by mechanical deformation. Sorby also discovered that steel can fracture through the crystals or along the boundaries between them; the microscopic details of fracture processes have never been clearly understood and are now under intensive investigation with new tools. The scanning electron microscope, a relatively recent innovation, is able to magnify surfaces 10,000 times or more so that the appearance of a broken piece of metal can be examined in great detail. Additional information about the micromechanics of fracture is provided by transmission electron microscopy, which can resolve elements of microstructure that are an order of magnitude smaller than those revealed by a scanning electron microscope. The heretofore obscure, but often large, effects of trace elements, and of minor differences in heat treating practices, are taking on new meanings because of the advent of these new tools of research.

#### THE PHASE RULE

The turn of the century marked the beginning of a new era in physical metallurgy. A series of important concepts and discoveries provided the foundation for the field of material science. One of the first, and most important, of these concepts was the phase rule, which Willard Gibbs

described in his famous paper published in the obscure journal of the Connecticut Academy in 1876<sup>3</sup>. However, the value of the phase rule was not widely recognized until about 1900<sup>4,5</sup>. Roozeboom<sup>6</sup> applied the phase rule of Gibbs to the study of steel, and published a classic metallurgical paper in 1900 which contained the iron-carbon equilibrium diagram. The phase rule provided a guiding principle which simplified experiments, provided a sound means for interpreting observations, and logically excluded an almost infinite number of possible explanations for the multitudinous, confusing observations that had resulted from microscopic examinations of steel specimens. Roozeboom<sup>7</sup> also made another valuable contribution to metallurgy. From thermodynamic considerations, he was able to show all of the general shapes of phase diagrams that binary alloys could be expected to exhibit, thus providing a sound basis for the classification of alloy systems.

#### DIFFUSION IN SOLIDS

Many of the reactions that take place in solid metals involve the process of diffusion. Early in the century it became obvious that solid state diffusion must be studied if reactions in solids were to be understood. This field of study became very active in the 1920's. Research on self-diffusion was conducted by von Hevesy<sup>8</sup>, who used radioactive isotopes as tracers. Methods were developed for measuring the diffusion coefficient,  $D$ , and Stefan<sup>9</sup> provided solutions to Fick's<sup>10</sup> law of diffusion (which had been derived by analogy from Fourier's law of heat flow). The mathematical solutions and experimental methods were applied by

Grube<sup>11</sup>, who showed that  $D$  varies with concentration. This led Matano<sup>12</sup> to apply Boltzmann's solution to the case of varying  $D$ .

The diffusion coefficient also varies with temperature. In 1920 von Hevesy<sup>13</sup> suggested that  $D$  varies exponentially with temperature, and in 1923, Dushman and Langmuir<sup>14</sup> showed that the temperature dependence was due to an activation energy process. Their equation,  $D = D_0 e^{-\Delta H/RT}$ , formalized the relationship between  $D$  and  $T$  (in this equation,  $D_0$  is a constant,  $\Delta H$  is the activation enthalpy,  $R$  is the ideal gas constant, and  $T$  is the temperature in  $^{\circ}K$ ).

#### CRYSTAL IMPERFECTIONS - VACANCIES AND DISLOCATIONS

Although the fact that atoms do move about in solids was established early in the century, the mechanism of the diffusion process was not clearly understood until about 1950. The general concept of crystalline solids was, and to a great extent still is, that atoms vibrate thermally about fixed lattice sites. In fact, however, atoms are able to move from one lattice site to another at temperatures above about half of the melting point (in  $^{\circ}K$ ). Several mechanisms of atom motion are possible. Atoms may interchange positions by the simultaneous motion of two, three, or four atoms moving in ring-like fashion. Detailed calculations have been made of these interchange processes, and although such motions are theoretically possible, the activation energies required for cooperative processes of this kind are much greater than experimental values of activation energy. Similarly, interstitial diffusion of atoms involves high energies, except for atoms much smaller than those that occupy lattice sites (e.g. carbon diffuses interstitially in iron).

When the assumption was made that crystals have vacant lattice sites, or vacancies, calculations of atom-vacancy interchange energies were found to be more consistent with measured energies. Many experiments have been made during the past several decades which show clearly that the vacancy--atom interchange process is the dominant mode of diffusion in metallic crystals.

In regard to the origin of vacant sites, the theory of vacancy generation is based on thermodynamic considerations. When an atom moves from the interior of a crystal to a position on the surface, its energy is increased. The number of bonds between atoms on the surface of a crystal is about half of the number for atoms in the interior. In face centered cubic crystals, for example, the number of bonds would thus decrease from 12 to 6. Since the energy of chemical bonds is of the order of 1/2 eV per bond (approximately 11,500 calories per mole), this simple estimate indicates that vacancy formation should require energy of the order of 3 eV. This estimate is high, however, because the atoms adjacent to a vacancy are displaced inward toward the center of the vacancy. This reduces the energy of the system by about 1 eV.

Atoms do not actually have to move out onto an exterior surface in order for vacancies to be generated. Vacancies can form spontaneously in a perfect lattice when local thermal fluctuations exceed the vacancy formation energy,  $E_v$ . The relative probability of an atom having an energy,  $E_v$ , greater than the ground state is  $e^{-E_v/RT}$ . The chance that an atom site will be vacant varies in the same way. In a crystal containing  $N$  atom sites, the number,  $n_v$ , of vacant sites is given by  $n_v = Ne^{-E_v/RT}$ .

Experiments have clearly shown that the number of vacant sites does vary in the exponential manner indicated by this equation.

The activation energy for diffusion in metals involves two terms, the one just described for vacancy generation, and a second exponential term containing the activation energy,  $E_m$ , for the movement of a neighboring atom into the vacant site. The sum of the two energies is the measured activation energy for diffusion,  $E_d$ .

There is a second type of crystal defect that plays a major role in controlling the properties of metals and alloys. It is called a dislocation, which is a linear discontinuity in the regular structure of a lattice. In its simplest form, a dislocation is the edge of an incomplete plane of atoms. Such defects can be generated by vacancies collecting together and replacing a sheet of atoms. Dislocations can also be formed by imperfect additions of atom planes to crystals that are growing during solidification. Mechanical deformation which produces a permanent change in shape of a piece of metal also generates dislocations within metal crystals. The number of mechanically produced defects may be very large, reaching  $10^{12}$  per square centimeter in severely deformed metals. The nature of this defect and its effect on the geometry of a lattice is illustrated in Fig. 1, which is a sketch of an edge dislocation. A second type of dislocation is sketched in Fig. 2, which shows how a defect can be introduced by shearing a crystal part way across. This type of defect is called a screw dislocation. Both types are commonly found in metals (by new techniques described in a subsequent section). The presence of dislocations in a crystal produces very high stresses

near the defects. Above the lower edge of the incomplete plane of atoms in Fig. 1, the atoms are closer together than their equilibrium distances, and a horizontal compression stress exists. Below the edge, the atoms are too far apart and the state of stress is tension. Also, high shear stresses are present on the horizontal planes perpendicular to the incomplete plane of atoms. A significant characteristic of both edge and screw dislocations is that when an external load is applied to a piece of metal, the stresses due to the load add to the stresses due to the presence of the dislocation. The forces between atoms become unbalanced, and the dislocation moves to a neighboring position, as shown in Fig. 3. With continued application of the external force, some dislocations move through crystals to external surfaces, producing "slip" offsets, as shown in Fig. 4. Other dislocations move shorter distances within crystals, eventually being stopped when they encounter boundaries between crystals in polycrystalline metals, or when they run into other dislocations that lie on intersecting crystallographic planes.

Metal crystals are inherently weak because dislocations can move easily through crystals under the action of relatively low externally applied loads. The way that metals are made strong is to block the motion of dislocations by introducing barriers to their motion, such as grain boundaries, other dislocations, or particles of a compound, such as  $\text{Fe}_3\text{C}$  in steel. Such compounds are, with few exceptions, strong and brittle. Dislocations cannot move through them, and unless the particles of the compound are very small and far apart, dislocations cannot move around them. The theory of dislocations is well advanced<sup>15,16</sup> and it is

possible to predict yield strength (the stress required to cause easily measurable amounts of permanent deformation, e.g. 0.2 pct) from a knowledge of the size and spacing of particles of the compound. Phase diagrams can be used to select alloys that will contain the desired quantity of a compound, and heat treatments can be selected that will provide the proper size and spacing of particles. Thus it is now possible to design alloys that will have prescribed yield strengths. Particle spacing, which is diffusion controlled, is only one of several important parameters that affect the mechanical properties of alloys. The others will be considered in later sections.

The history of dislocation theory is interesting because dislocations were conceived to explain the observed mechanical behavior of metals in 1934. Their existence was not experimentally verified by direct observation until 1955, when they were first seen by means of transmission electron microscopy. In the 1920's calculations were made of the theoretical yield strengths of pure metal crystals. Plastic flow involves the sliding of close packed planes of atoms over one another. The shear stress,  $\tau_y$ , required to cause all atoms in a plane to move simultaneously is approximately equal to one-tenth of the shear modulus of elasticity,  $G$ . The shear modulus of iron is  $11 \times 10^6$  pounds per square inch (psi), so the shear stress required to start permanent deformation should be about  $10^6$  psi. The measured yield strengths were actually less than 100 psi. In view of the large discrepancy, Taylor<sup>17</sup> and Orowan<sup>18</sup> independently arrived at the conclusion that the low strength of real crystals was caused by some type of crystal imperfection. The type that met the

mathematical requirements was the edge dislocation. Burgers<sup>19</sup>, in 1939, showed that the screw dislocation also satisfied the conditions leading to plastic flow at low stresses. The theory of dislocations was looked upon with skepticism for about 15 years, then more sophisticated analyses were gradually developed and confidence in the theory became more widespread. By the early 1950's the theory was generally accepted, but direct and convincing proof of its validity was still lacking. In 1952, boundaries between two slightly mis-oriented crystals were observed to move with stress<sup>20</sup>. These boundaries were made up of arrays of parallel edge dislocations, all lying in the boundary. This was the first observation of groups of dislocations moving in stressed crystals. By 1955, transmission electron microscopy had advanced to the stage where images of single dislocations could be seen and photographed<sup>21</sup> in motion in metal crystals. Transmission microscopy had opened a new era of research in materials science. The behavior of dislocations was found to be much more complicated than the simple theoretical pictures indicated. They were observed to be curved, tangled, and to interact with each other in complex ways. An accurate understanding of the properties of dislocations and how they react with each other, with the boundaries between crystals, and with precipitated particles of metallic compounds, evolved during the decade following the first observations. Progress has been so great that it is now possible to use dislocation theory for the quantitative design of new alloys. This theoretical area has nearly reached maturity, but other critical areas remain in primitive stages of development. Among those requiring additional attention are non-equilibrium chemical reactions that occur in solids, particularly in steels.



## SOLID STATE CHEMICAL REACTIONS

The equilibrium decomposition products of the high temperature solid solution phase of steel should be pure body centered cubic iron and graphite. These products are never actually found in steel. Instead of graphite,  $\text{Fe}_3\text{C}$  forms when the steel is slowly cooled, and when steel is quenched rapidly to room temperature, a single body centered tetragonal phase forms. The latter phase is called martensite. It is a highly supersaturated solution of carbon in body centered cubic iron and it is nearly as brittle as glass. When martensite is reheated to about  $200^\circ\text{C}$ , carbon precipitates out of the iron, but not as graphite or  $\text{Fe}_3\text{C}$ . A compound called epsilon carbide, with the formula  $\text{Fe}_2\text{C}$ , forms. This phase has a hexagonal crystal structure and is semicoherent with the iron lattice (i.e., atoms on some planes of the two phases match geometric arrangements so that no definite boundary is formed). When quenched steel is heated above  $200^\circ\text{C}$ , epsilon carbide redissolves and the orthorhombic  $\text{Fe}_3\text{C}$  phase appears. The epsilon carbide forms as tiny plates, observable only with an electron microscope. The  $\text{Fe}_3\text{C}$  particles that appear after higher temperature heating first appear as small sheets, but soon assume approximately spherical shapes, as shown in Fig. 5. The higher the reheat temperature, the larger the carbide particles become and the fewer of them there are. Being farther apart, they interfere less with the motion of dislocations. Therefore, the room temperature yield strength decreases with increasing reheat temperature, as shown in Fig. 6.

When steel is slowly cooled from a high temperature (e.g.,  $900^\circ\text{C}$ ),  $\text{Fe}_3\text{C}$  and body centered cubic iron form by an eutectoid reaction. In this

case, the  $\text{Fe}_3\text{C}$  is in the shape of plates, as shown in Fig. 7. The shape of the  $\text{Fe}_3\text{C}$  particles has a profound effect on the mechanical properties of steel, with the ductility being much less when  $\text{Fe}_3\text{C}$  is present as plates instead of spheres. This is illustrated by the results of tests in which two cylindrical bars of steel containing 0.3 pct C are broken by a tensile load. When such bars are pulled apart, they increase in length and reduce in diameter. In an actual test, the cross sectional area of a bar with spherical carbide particles was reduced by 70 pct before the bar broke. The same steel, heat treated to cause  $\text{Fe}_3\text{C}$  to form as plates, only reduced 35 pct in area. Both bars had the same yield strength, namely 60,000 psi, but their fracture strengths, as well as their ductilities, differed greatly. This example is cited to illustrate the importance of controlling the morphologies of the microconstituents of steels. In addition to the shape of carbide particles, there are other important microstructural features that must be controlled in order to endow steels with optimum properties for specific applications.

#### ISOTHERMAL DECOMPOSITION OF AUSTENITE

At temperatures above about  $900^\circ\text{C}$ , steels exist as a single phase, a solid solution of carbon in face centered cubic crystals of iron. This phase is called austenite. As mentioned earlier, when a steel is cooled slowly, a plate-like eutectoid structure, called pearlite forms, and when a steel is quenched rapidly to room temperature, a metastable body centered tetragonal phase, highly supersaturated with carbon, is produced. The latter phase is called martensite. Pearlite and marten-

site have been known to exist for a long time. However, early investigators found that in many alloy steels (i.e., steels containing other alloying elements in addition to carbon), microstructures not found in carbon steels frequently appeared. Even with carbon steels, mysterious events sometimes occurred. In quenched steels, pearlite would sometimes be present, but at other times it would not, even when the heat treating procedures remained constant. To determine the reasons for variations in microstructural appearance, Bain<sup>22,23</sup> and his coworkers performed experiments in 1929 in which austenite was made to decompose isothermally instead of during continuous cooling. They quenched small pieces directly into molten lead baths held at fixed temperatures below the equilibrium transformation temperature. Two methods were used to monitor the changes that occurred in the internal structure. One method involved continuous length change measurements (approximately 1 pct increase occurs when the crystal structure transforms from face centered to body centered cubic). The second procedure was to observe differences in microstructures of pieces that were removed from the lead bath at various time intervals and quenched in cold water. The fraction of the volume that had not transformed in the lead bath was converted to martensite during the quench. In the portion that had transformed carbides were precipitated. The areas containing carbide particles appeared dark when viewed under a microscope, in contrast to areas of martensite which were much lighter in appearance.

The austenite decomposition rate varied substantially with the holding temperature, as shown in Fig. 8. At the higher temperatures, pearlite

formed. At low temperatures and on rapid cooling, austenite was found to transform instantaneously to martensite. In the intermediate temperature range, a new microstructure formed. This structure was dark in appearance and resembled martensite that had been reheated to a low temperature (where carbides precipitated as small particles). However, recent transmission electron microscopy studies have shown that the new structure and reheated martensite differed in detail, and also that not one, but two, distinctly different structures form in the intermediate temperature range. These two microstructures have been named upper and lower bainite, in honor of their discoverer Bain.

It had been recognized for a decade before Bain's work that the addition of alloying elements, such as chromium, molybdenum, and nickel, increased the "hardenability" of steels--that is the ability of steel to harden to a greater depth than plain carbon steel when quenched from the austenite state. The effect of such additions is shown in Fig. 9 for a steel containing 0.40 pct C, 1.75 pct Ni, 0.80 pct Cr, and 0.25 pct Mo (AISI 4340 steel). Comparisons of Figs. 8 and 9, show that the pearlite reaction can start in as short a time as 1 sec in the 0.80 pct C steel, whereas the same reaction in the AISI 4340 alloy steel does not begin before about 150 sec. Similarly, the bainite reaction, which takes place in the temperature range 540° to 260°C, starts in 1 sec at 540°C and in about 200 sec at 260°C in the 0.80 pct C steel. The behavior of the alloy steel is much different in the bainite range. The reaction is very slow, starting after 20,000 sec at 540°C and in 10 sec at 260°C.

The time-temperature-transformation curves shown in Figs. 8 and 9 are called TTT diagrams. During the 20 years following Bain's pioneering work, a great deal of effort was devoted to evaluating the effects of alloying elements on the decomposition kinetics of austenite and the morphologies of the decomposition products. Many TTT diagrams were published, but no basic laws of behavior were ever resolved; TTT diagrams have remained empirical in nature; it is still not possible to predict the shape of a TTT diagram of a steel containing several alloying elements selected at random. By 1950 interest in attempts to rationalize the alloying effects had diminished to a negligible level. Practically no new TTT diagrams have appeared in the literature since then. One of the reasons for the decrease in interest was that accurate diagrams had been experimentally determined for all the important alloy steels. Another was the time consuming nature of such determinations. About one month of concentrated work was required to produce a single diagram, and it seemed to most researchers that their efforts could be better devoted to work on more urgent problems. Thus there remains today the challenge to solve the solid state chemistry problem of discovering the basic laws that govern the decomposition kinetics of austenite in alloy steels. A concerted effort on this problem is now underway in the Center for the Design of Alloys in the Inorganic Materials Research Division of the Lawrence Berkeley Laboratory at the University of California. The number of possible combinations of useful alloying elements (e.g., Cr, Ni, Mo, Mn, Si, Co, V, Ti, W, Nb, Cu and others), in varying concentrations, is extremely large. The only possible hope of obtaining sufficient

quantitative data about the synergistic effects of the alloying elements is to devise a rapid method for measuring their effects on austenite decomposition kinetics in the bainite temperature range (which has been established as the range most important in determining mechanical properties). It has been found that magnetic susceptibility, monitored continuously, can be used to measure the amount of the ferromagnetic body centered cubic phase of iron as it forms from the face centered cubic austenite. With this method, the important part of a TTT diagram can now be established in a single day. Furthermore, the magnetic method is so sensitive that it has been possible to establish that upper bainite and lower bainite reactions follow two independent C-shaped curves, as shown in Fig. 10. New research in this old field is turning out to be unusually rewarding. It is leading to discoveries that we believe will make possible the design of a new group of high strength alloys--steels that will have considerably greater fracture toughness (i.e., the resistance to fracture when sharp cracks are present) than the ones now in use.

#### TRANSMISSION ELECTRON MICROSCOPY

Quantitative evaluations of the factors that control the kinetics of decomposition of austenite must be evaluated before new steels can be discovered or designed, but TTT diagrams provide only part of the required information. The shapes and distributions of the phases resulting from the decomposition of austenite vary over a wide range. Carbides vary in shape from finely divided particles that are uniformly distributed in body centered cubic iron, to thin films surrounding crystals free from

carbides. The ductility of steel is highly sensitive to microstructural variations. When carbide films are present, the steel may be almost as brittle as glass. By contrast, when the carbide particles are small, separate, and uniformly distributed, the steel will tear apart slowly when loaded to failure. The nature of a microstructure cannot be predicted from a cooling curve and a TTT diagram. Consequently, the microstructure of every new alloy must be determined by a microscopic examination after each variation in heat treating procedure. The best method for producing a microstructure that will resist brittle fracture is not yet predictable from principles of materials science, but progress is being made toward a solution of this problem.

There are several microstructural features that are known to meet the theoretical requirements (based on dislocation mechanics) for high strength combined with good toughness. One of these requirements is that the mean free path for dislocation motion must be small, preferably much less than a micron. Dislocations on slip planes pile up at barriers, each adding to the stress concentration at the barrier. The number of dislocations on a single slip plane varies as the square root of the distance between barriers. The local stress at the front of a pile-up is equal to the number of dislocations times the average stress produced by the externally applied load. When the local stress at the head of the pile-up reaches the cohesive strength of the crystal, a microcrack forms. These microcracks grow and eventually join, causing general rupturing of the material. One way to increase the strength and toughness simultaneously is to make the grain size very small. Grain boundaries act as

barriers to dislocations, and small grains reduce the dislocation mean free path, enhancing both strength and toughness. An example of how grain size control can be used to produce a potentially useful alloy is given in the following section.

#### DESIGN OF A CRYOGENIC ALLOY HAVING HIGH TOUGHNESS

Metals or alloys with the body centered cubic structure can fail either by shear, as in face centered cubic metals, or by cleavage. It is now well established that the propensity of body centered cubic metals to fail by cleavage is influenced by a host of compositional and structural factors. Some of the compositional and microstructural features that are desirable in a body centered cubic cryogenic alloy are: (1) the lowest possible level of interstitials in solid solution (interstitials raise the critical resolved shear stress of body centered cubic metals to the cleavage stress as the temperature is lowered), (2) the maximum amounts of either nickel or manganese in solid solution commensurate with other metallurgical considerations, and (3) the finest possible grain size. This listing of desirable features is, of course, not complete and is intended only as a guide for the selection of an alloy system for study. Iron-rich alloys in the Fe-Ni-Ti system meet the requirements cited above. The titanium and nickel contents in these alloys can be varied to meet the requirements (1) and (2) above. Fine grain sizes can be obtained by thermal or thermal-mechanical means. In the study discussed below, the requirements (1) and (2) were met by the alloys Fe-12 pct Ni-0.5 pct Ti and Fe-12 pct Ni-0.25 pct Ti\* . After initial processing

\*All chemical compositions are in wt pct except where otherwise indicated.



and forming into desired shape, the alloys were solution annealed for 2 hr, air cooled to room temperature, then reheated to a designated temperature between 650°C and 800°C, and ice brine quenched.

The results of grain size and impact studies are shown graphically in Fig. 11. There was not a simple relationship between the phase diagram and the heat treatments required for grain refinement. Current studies suggest that the refinement is produced by an increase in the nucleation rate of the prior austenite ( $\gamma$ ) grains above the two phase ( $\alpha+\gamma$ ) region. Apparently the residual defect structure remaining from the duplex ( $\alpha+\gamma$ ) microstructure provides the additional nuclei. The temperatures for effective grain refinement were between about 675°C and 775°C, as can be seen in Fig. 11(a).

The -196°C Charpy V-notch impact energies of both alloys reheated for 2 hr at temperatures indicated are shown in Fig. 11(b). The impact energies were uniformly high for reheating temperatures between 675°C and 775°C, and low for temperatures on either side of this range. It was noted that fine grain size and high impact energies were both obtained for the same reheat temperatures. Correlations such as these were not possible for room temperature tests because of the limited capacity of the testing machine (225 ft lbs).

Macrographs of the broken Charpy V-notch bars, optical photomicrographs of the microstructure showing the grain size, and scanning electron micrographs of the fracture surface of the Fe-12Ni-0.5Ti alloy are shown in Fig. 12 for several reheat temperatures. It is readily apparent that there was a correlation between the grain size and the macro- and

micro-fracture appearance. Specimens having a fine grain size showed gross amounts of plasticity on the fracture surfaces of the broken Charpy bars. Their fracture surfaces at high magnification exhibited dimpled rupture that is characteristic of shear (high energy) failure. On the other hand, specimens having a large grain size showed little plasticity on the fracture surface of the Charpy bars and their fracture surfaces at high magnification were characterized by flat facets indicative of cleavage (low energy) failure.

The effect of the time of reheat on toughness is shown in Fig. 13 for temperatures between 650°C and 800°C. The energy absorbed at -196°C was clearly a function of both temperature and time. The grain size in microns is shown in parentheses on the curves in Fig. 13. At the reheat temperature of 650°C, the energy absorbed did not appreciably vary from its initial low value for times up to 30 hr. At the highest reheat temperature of 800°C the energy absorbed reached a low peak in about 1/2 hr and then decreased with time to a relatively low value. At intermediate temperatures, viz, 700°C and 750°C, the impact energy rose rapidly as a function of time to high values and did not change for times up to 6 hr. As shown in Fig. 13 there was a corresponding reduction in grain size with time for specimens treated in the intermediate temperature region. This time-temperature-grain size relationship was especially evident for those specimens reheated at 700°C.

The -196°C impact toughness and yield strength of the Fe-12Ni-0.5Ti alloy are compared in Fig. 14 with those reported in the literature for two commonly used commercial cryogenic steels<sup>25</sup>. The superior combination

of strength and toughness of the new alloy is clearly evident. The Charpy V-notch impact properties at liquid helium temperatures were in excess of 100 ft lbs.

Some typical tensile results are shown in Table 1 for test temperatures of 23°C and -196°C. The tensile properties were quite insensitive to the reheat temperature. It is apparent that those microstructural features which influence the impact toughness did not appreciably affect the tensile properties. In tests at near liquid helium temperatures (-266°C) higher yield and tensile strengths were observed with no appreciable decrease in ductility. The tensile properties of the Fe-12Ni-0.25Ti alloy were similar to those of the Fe-12Ni-0.5Ti alloy, although the strength was somewhat lower (about 5 pct) at all test temperatures. (For additional details see references 26-31).

TABLE 1. Tensile Properties of the Fe-12Ni-0.5Ti Alloy

2 Hour Reheat at 750°C					2 Hour Reheat at 850°C			
Test Temp., °C	*Yield Strength, ksi	Ultimate Tensile Strength, ksi	Elong., pct	Red. in Area, pct	*Yield Strength, ksi	Ultimate Tensile Strength, ksi	Elong., pct	Red. in Area, pct
23	90.3	98.6	21	84	90.8	98.3	21	86
-196	139.5	153.0	18	75	140.0	150.5	21	74

\*0,2 pct offset

DESIGN OF A NEW ALLOY FOR ELEVATED TEMPERATURE SERVICE

At ambient and cryogenic temperatures, most metallic materials exhibit a plastic strain only when subjected to a stress higher than the yield

strength, and then the strain does not vary with time. However, at elevated temperatures, metals and alloys experience a time dependent plastic deformation process at stresses below the yield strength. Such a process leads to adjustments in the internal structure of a deformed metal causing an increase in strain as a function of time at a constant load and temperature. Time dependent deformation of this nature, known as creep, adds a new dimension to the mechanical behavior of alloys at elevated temperatures. Design of alloys for elevated temperature applications is complex because of the need to design for creep resistance.

Most commercial creep resistant materials derive their strength from a fine dispersion of a second phase which hinders the movement of dislocations. In creep resistant ferritic steels, the fine dispersion almost invariably consists of carbides, whereas in high nickel content superalloys, the dispersed phase may be an intermetallic compound such as  $\text{Ni}_3(\text{Al},\text{Ti})$ . The particle size, morphology, distribution and volume fraction of the second phase, the degree of its coherency with the matrix, and the mechanical properties of the matrix all affect the creep resistance of dispersion strengthened alloys. The thermal stability of the second phase particles is also an important factor.<sup>32</sup>

The morphology and composition of carbide particles tend to change slowly at elevated temperatures and this often results in an increase in creep rate. An example of such an effect is the loss in creep strength of 0.1C-1.0Cr-0.5 Mo steel after long time exposure at service because of the formation of an  $\text{M}_6\text{C}$  type of carbide,<sup>33</sup> where M is a combination of metal atoms.

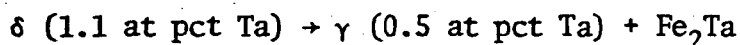
The concept of using intermetallic compounds, rather than carbides, for increasing the high temperature strength of alloys is decades old, but progress toward a realization of this concept has been slow. The effects of intermetallic compounds such as the sigma phase and  $\text{Ni}_3(\text{Al},\text{Ti})$  have been investigated by Mihalisin, et al<sup>34</sup> and Decker.<sup>35</sup> Mihalisin et al<sup>34</sup> found that the presence of sigma lowered both stress-rupture and room temperature strengths. Decker<sup>35</sup> also summarized the status of knowledge about the effects of the Laves phase (an intermetallic compound which requires a specific atomic size ratio between its components) particles on strength. He concluded that in general, when the Laves phase is present in significant amounts it "...can degrade room temperature ductility with little effect on creep properties". The results from the present investigation showed, however, that with microstructural control, satisfactory values of room temperature strength and ductility, as well as good stress-rupture life, can be attained in very low carbon alloys strengthened with the Laves phase  $\text{Fe}_2\text{Ta}$ .

Recently it was demonstrated by Jones, et al<sup>36</sup> that in body centered cubic Fe-Ta alloys, the brittleness, which was due to the presence of a continuous grain boundary network of the Laves phase  $\text{Fe}_2\text{Ta}$ , could be overcome by a simple heat treatment which spheroidized the precipitate. Spheroidization of the Laves phase resulted in considerable enhancement of room temperature ductility and elevated temperature strength of Fe-Ta alloys. Two major limitations of Fe-Ta alloys with respect to their possible practical utilization for elevated temperature service were:

- (1) the high  $\alpha \rightarrow \gamma$  and  $\gamma \rightarrow \delta$  phase transformation temperatures that

necessitated high temperature heat treatments, and (2) inadequate oxidation resistance. An examination of the binary Fe-Cr phase diagram<sup>37</sup> indicated that increasing chromium additions to iron continuously lower the  $\gamma \rightarrow \delta$  phase transformation temperatures. The  $\alpha \rightarrow \gamma$  transformation temperature, on the other hand, is lowered by chromium additions of up to 7 pct, but is raised by further additions of chromium. It seemed reasonable to expect that qualitatively, a similar trend would be observed on addition of chromium to Fe-Ta alloys. Also, it is well known that improvements in oxidation resistance are not obtained in ferritic alloys until about 7 pct chromium is present.<sup>38,39</sup> The above consideration led to the development of a ternary Fe-1 at pct Ta-7 at pct Cr alloy (hereafter referred to as alloy Ta7Cr).

The Fe-rich portion of the equilibrium phase diagram<sup>40</sup> of the Fe-Ta system is shown in Fig. 15. There are three solid solution regions,  $\alpha$  (bcc),  $\gamma$  (fcc) and  $\delta$  (bcc). The intermetallic compound,  $\text{Fe}_2\text{Ta}$ , is a Laves phase, and it has a hexagonal structure. The  $\delta$  phase decomposes by a eutectoid reaction at 1239°C in accordance with:



The  $\gamma$  phase reacts with  $\text{Fe}_2\text{Ta}$  in a peritectoid reaction at 972°C to produce the  $\alpha$  solid solution:



Chromium additions change the compositions and temperatures of these transformations,<sup>41</sup> as shown in Table 2. The  $\alpha \rightarrow \gamma$  and  $\gamma \rightarrow \delta$  transformation temperatures listed in Table 2 were obtained by dilatometry, and

the  $(\gamma + \delta) \rightarrow \delta$  and  $(\text{Fe}_2\text{Ta} + \delta) \rightarrow \delta$  temperatures were determined by metallography.

TABLE 2. Phase Transformation Temperatures for Fe-Ta-Cr Alloys

Alloy Composition	Phase Transformations and Temperatures ( $^{\circ}\text{C}$ )		
	$\alpha \rightarrow \gamma$	$\gamma \rightarrow \delta$	$\gamma + \delta \rightarrow \delta$ or $\text{Fe}_2\text{Ta} + \delta \rightarrow \delta$
Fe-1 at pct Ta	974	1238	1340
Fe-1 at pct Ta-3 at pct Cr	890	1230	1300
Fe-1 at pct Ta-5 at pct Cr	880	1210	1280
Fe-1 at pct Ta-7 at pct Cr	870	1160	1250

The structure of the alloy Ta7Cr in the solution treated (for 1 hr at  $1320^{\circ}\text{C}$ ) and water quenched condition was characterized by large grains (approximately 1 mm in average diameter) of the retained  $\delta$  phase, and by an almost continuous grain boundary network of precipitate. When the alloy was aged at  $700^{\circ}\text{C}$ , additional precipitate formed within the grains, but there was no noticeable change in the grain boundary network. Microhardness measurements on samples aged for several time intervals at  $700^{\circ}\text{C}$  showed that the hardness first increased with increasing aging time, reached a maximum after 40 minutes of aging, and then decreased. The microstructure of the alloy in the peak hardness condition is shown in Fig. 16(a). When the aged alloy was heated to  $1100^{\circ}\text{C}$ , the matrix transformed to the face centered cubic solid solution, and the grain boundary precipitate spheroidized. On cooling from the  $\gamma$  phase field, the matrix again transformed to body centered cubic  $\alpha$ , with a consequent refinement in grain size. The structure after this treatment consisted of spheroid-

ized precipitate particles in a matrix of  $\alpha$  which was characterized by irregular grain boundaries, as shown in Fig. 16(b). In Fig. 17 is shown a transmission electron micrograph of a carbon extraction replica showing a uniform distribution of almost spherical particles of the Laves phase in the spheroidized alloy.<sup>42</sup>

The tensile properties of the Ta7Cr alloy, after aging at 700°C for 40 minutes were characterized by yield and ultimate tensile strengths which decreased very gradually with increase in test temperature up to about 600°C; at this temperature the 0.2 pct offset yield strength, (i.e., the stress to cause a permanent deformation of 0.2 pct) was about 70 pct of the room temperature value. The room temperature fracture was brittle as indicated by the scanning electron fractograph shown in Fig. 18(a). The room temperature fracture behavior was changed from brittle to ductile by the spheroidizing heat treatment that followed aging. The fracture surface of the tensile specimen tested at room temperature after spheroidizing at 1100°C for 10 minutes is shown in Fig. 18(b). In this figure, there is evidence of a significant amount of plastic deformation, as indicated by a dimpled appearance. Fracture occurred by void nucleation and growth at the interfaces between  $\text{Fe}_2\text{Ta}$  particles and the matrix. The yield strength, tensile strength, and fracture elongation are plotted as a function of the test temperature in Fig. 19 for the alloy in spheroidized condition. The results were similar to those of the alloy in the aged condition except that all the mechanical properties were increased in the spheroidized alloy. The improvements were attributed to the combined effects of spheroidization of the grain boundary precipitate, reduction in grain size, and an increase in dislocation density.



Short time tensile properties do not provide adequate information about high temperature strength, and so stress-rupture tests were made on the Ta7Cr alloy. The temperatures selected for evaluation were 1000°F (538°C) and 1100°F (593°C). Stress vs time to rupture data for 1100°F (593°C) are plotted in Fig. 20. Also shown in the figure are the stress-rupture properties reported in the literature for 0.3C-1Cr-1Mo-0.25V steel, 0.15C-9Cr-1Mo steel, Greek Ascoloy and 403, 410 and 422 stainless steels.<sup>43</sup> At 1100°F (593°C), the Ta7Cr alloy results were above those reported for the 0.15C-9Cr-1Mo steel, and 403 and 410 stainless steels, but below those for the Greek Ascoloy, 422 stainless steel and the 0.3C-1Cr-1Mo-0.25V steel.

The strengthening effect of molybdenum in solid solution in ferrite is well known<sup>44-46</sup> so 0.5 at pct of molybdenum was added to the Ta7Cr alloy, and the alloy Ta7CrMo was developed. The expected strengthening was found when stress-rupture tests were performed at 1100°F (593°C) on the Ta7CrMo alloy. The results are shown in Fig. 20. Additional detailed information on this study is reported elsewhere.<sup>42,47-49</sup>

#### DESIGN OF STRONG, TOUGH STEELS FOR USE AT AMBIENT TEMPERATURES

The resistance to sudden and catastrophic failure is one of the most important design requirements of engineering structures. Until the advent of modern fracture mechanics, there was no known quantitative way to associate the microstructure of an alloy with its tendency to fail catastrophically. Earlier tests, such as the Charpy, do not provide quantitative design data. The pioneering work of Irwin, et al in the late fifties has resulted in a totally new approach to the problems of fracture

of complex engineering structures. As is now well known, the intrinsic fracture toughness of certain alloys can be quantitatively evaluated in terms of a stress intensity factor,  $K$ , with  $K_C$  being the stress intensity required for the catastrophic propagation of a crack in a sheet of material subjected to plane stress, and  $K_{IC}$  being the parameter for the plane strain state. Of particular interest to the materials scientist is the observation that both  $K_C$  and  $K_{IC}$  are highly dependent on internal structure. The development of a quantitative approach to fracture has provided a vital link between materials science and materials engineering. The materials scientist can hence use his knowledge of defect structure and microstructure to produce alloys with enhanced resistance to fracture. The mathematical formalism of modern fracture mechanics has also been applied to the problem of fracture by fatigue, but the quantitative correlation between fatigue failure and microstructure is not as well understood, as is catastrophic fracture.

The evolution of a unified theory of fracture mechanics and the development of reliable test methods for obtaining an accurate value for the plane strain fracture toughness ( $K_{IC}$ ) have provided the metallurgist with a quantitative method for evaluating the effects of microstructural details on the tendency of an alloy to fracture in a brittle manner. Studies of the relationship between the microstructure and the fracture toughness of ultra high strength steels have been especially rewarding. For example, the deleterious effects of sulfur and other trace impurities have been quantitatively determined.<sup>50,51</sup> Also, the relative merits of steels with bainitic, martensitic, or tempered martensitic microstructures have been well documented with respect to their strength and

fracture toughness.<sup>52-54</sup> Steels are often rated according to their relative positions on master plots of plane strain fracture toughness vs yield strength.<sup>55</sup>

The assumption is generally made that the high hardenability of commercial quenched and tempered steels leads to uniform microstructures throughout the thickness of fracture toughness specimens, because the hardness is nearly constant throughout the thickness. Elementary considerations of micromechanics of fracture lead to the conclusion that the fracture toughness of ultra high strength steels should be highly dependent on relatively small amounts of embrittling microconstituents, whereas such microconstituents have little effect on the hardness. The detection of minor amounts of austenite decomposition products by either optical or electron microscopic techniques is deceptive in its apparent simplicity. The detection by optical microscopy, for example, of small amounts (of the order of 1 pct) of upper bainite in a 5/8 inch thick specimen consisting largely of lower bainite or autotempered martensite demands the utmost care and patience in all stages of specimen preparation. It is now established that high resolution electron microscopy is needed to distinguish between lower bainite and autotempered martensite. Unfortunately, the advantages of electron microscopy are offset by the disadvantage that large areas cannot be scanned readily. A combination of metallographic techniques is generally the most effective way to study the structures of heat treated steels. When metallographic techniques reveal the presence of embrittling structures in conventionally heat treated steels, alternate heat treatments should be devised to either

eliminate, or at least minimize, such structures.

Recent studies on a secondary hardening 5 Mo-0.3 C steel have suggested one way in which improvements in microstructural uniformity can be achieved.<sup>56-58</sup> Increases in fracture toughness of more than 50 pct were obtained in as quenched specimens by the use of high austenitizing temperatures. In this case, the improvement was attributed to the reduction of undissolved alloy carbides. In the present investigation several commercial steels were heat treated at different austenitizing and tempering temperatures and their strength and fracture toughness determined. The results obtained are reported herein.

The compositions and properties of the steels used in the present investigation are shown in Table 3. Specimens for optical and electron microscopy were taken from the fracture toughness specimens which had been designed and tested in accordance with ASTM recommended practices.<sup>59</sup> Sufficient sampling was done to ensure that representative microstructures were obtained.

The effect of austenitizing temperature on the fracture toughness of as quenched specimens of the 5 Mo-0.3 C steel is shown in Fig. 21. The abrupt increase in fracture toughness at a critical austenitizing temperature was associated with an increase in grain size (ASTM 7-8 to 1); the grain size change was concomitant with complete solution of the alloy carbides.

Several different microstructural features were responsible for the lower fracture toughnesses of the three steels when they were austenitized at the conventionally used temperature (870°C). The optical micrographs of AISI 4130 steel, oil quenched from 870°C, clearly showed grains

TABLE 3. Austenitizing and Tempering Temperatures, Fracture Toughness and Yield Strength of 5 Mo-0.3C, AISI 4130 and AISI 4340 Steels

Steel (Composition in wt pct)	Austenitizing Temperature, °C	Quenching Medium	Tempering Temperature, °C	Yield Strength (0.2 pct offset) ksi	Fracture Toughness, ksi-in <sup>1/2</sup>
5Mo-0.60Mn-0.30C (Laboratory heat)	870	Iced Brine	As Quenched	194	52
	1200	Iced Brine	As Quenched	214	100
	1200	Iced Brine	150	210	104*
	1200	Iced Brine	225	196	109*
AISI 4130 (0.30C-0.85Cr- 0.46Mn-0.20Mo) (Commercial steel)	870	Oil	As Quenched	201	57
	1200→870**	Oil	As Quenched	210	73
	1200	Iced Brine	As Quenched	214	100
	1200	Iced Brine	200	210	110
AISI 4340 (0.40C-0.72Cr 1.73Ni-0.80Mn- 0.24Mo) (Commercial steel)	870	Oil	As Quenched	231	35
	1200→870**	Oil	As Quenched	231	63
	870	Oil	200	235	62
	1200→870**	Oil	200	230	75

\*K<sub>Q</sub>, rather than K<sub>IC</sub>, values.

\*\*Specimens cooled slowly from 1200°C to 870°C before quenching to maintain quenching conditions identical with 870°C austenitized specimens.

of ferrite and many regions of upper bainite.<sup>60</sup> The remainder of the structure was identified by transmission electron microscopy as being lower bainite and autotempered martensite. When the austenite grain size was increased by first heating the steel to 1200°C (then furnace cooled to 870°C before oil quenching), there were no ferrite grains visible in the optical micrograph, and the amount of upper bainite was substantially lower than that formed during the direct quench from 870°C. The fracture toughness was increased about 30 pct by the 1200°C treatment.<sup>58</sup>

Free ferrite grains and ferrite plates in upper bainite are regions that are mechanically weak. They can fail readily by either plastic flow or by cleavage, and thus they tend to initiate microcracks at relatively low levels of plastic strain. This results in low values of fracture toughness, even when dimpled rupture occurs, as scanning electron microscopy revealed was the case for this steel. In additional experiments, fracture toughness specimens were quenched into iced brine directly from 1200°C. The cooling rate in this case was fast enough to suppress the formation of upper bainite, although small amounts of a bainitic product were visible in isolated regions in optical micrographs. The remainder of the microstructure appeared to be autotempered martensite. Specimens given the iced brine quench had exceptionally high fracture toughness (100 ksi-in.<sup>1/2</sup>):

Another microstructural feature that can have a marked influence on fracture toughness is retained austenite. The presence of austenite films has been observed by other investigators, and there has been some speculation about its influence on toughness.<sup>61-63</sup> However, in martensitic steels it is generally assumed that no retained austenite exists if

no evidence for fcc reflections can be obtained by x-ray diffraction. Since standard x-ray methods have a resolution limit of approximately 1 pct, and since the morphological distribution of austenite needs to be characterized it is necessary to utilize transmission electron microscopy and diffraction. Proof of the existence of very thin films (approximately 200 Å thick) of austenite at martensite lath boundaries was first obtained in studies of Fe-Cr-C steels.<sup>64</sup> In the case of AISI 4340 steel, the presence of retained austenite in oil quenched specimens with the larger austenite grains appeared to markedly enhance the fracture toughness.<sup>58</sup> Optical micrographs did not reveal the structural nature of this steel in any of the conditions investigated. Transmission electron microscopy and diffraction showed that the structure was primarily autotempered martensite with small amounts of lower bainite and untempered martensite for both the 870°C, and the 1200° to 870°C austenitizing conditions. The only significant difference observable in the two steels was that austenite films, 100 to 200 Å thick, surrounded a majority of the martensite laths in the specimens that had been heated to 1200°C, as can be seen in the dark field electron micrograph of Fig. 22, whereas there was only a trace of retained austenite visible in the specimens heated to 870°C. Additional diffraction and dark field microscopy showed that the retained austenite did not transform when specimens were cooled to liquid nitrogen temperature.

Austenite is not sensitive to high local stress concentrations and does not fail by cleavage, as does ferrite. Consequently, it seemed reasonable to conclude that in this case, the presence of another phase, properly dispersed, can actually enhance the fracture toughness.

As is predictable from basic principles of materials science, low fracture toughness of a quenched and tempered steel is associated with the presence of certain types of microstructural features. Sulfide inclusions act as microcrack nuclei and therefore induce macrofracture at relatively low strains in fracture toughness specimens. Similarly, carbide particles undissolved during austenitizing lower toughness. Free ferrite, whether present as separate grains or as platelets in upper bainite in ultra high strength steels, lowers fracture toughness by a substantial amount.

Autotempered martensite (with no interlath carbides) formed during the quenching operation is tough. Lower bainite, and tempered martensite free from lath boundary films of carbides, are also tough and fracture resistant microstructural constituents. The presence of retained austenite films around autotempered laths of martensite adds substantially to the inherent toughness of the autotempered martensitic structure. The substructure of martensite itself is also important, e.g. transformation twinning in carbon steels lowers toughness.<sup>52</sup>

Figure 23 summarizes the results of tests on steels that had been given the 1200°C austenitizing treatment. The fracture toughness,  $K_{IC}$  is plotted against the yield strength. In this figure there are two bands which show the ranges of yield strength and fracture toughness values reported in the literature for commercial AISI 4340 steel and the 18 Ni maraging alloy. The maraging steels are usually considered to have the highest value of plane strain fracture toughness obtainable at a given yield strength. The circles are test points for steels given special heat treatments described herein. The toughness values have been moved out of



the lower and into the upper band. Furthermore, there are theoretical reasons to believe that fracture toughnesses well above the maraging steel band can be obtained with quenched and tempered steels through modifications of chemical composition and thermal treatments.

Figure 24 shows the approximate range of results obtained with TRIP steels<sup>65-68</sup> and how the fracture toughness values compare with those of quenched and tempered, and maraging steels. The TRIP steels are metastable austenitic ultra high strength steels that transform martensitically when plastically deformed. These steels contain 0.3 pct carbon or more, and the strain-induced martensite formation provides an additional strengthening mechanism. A volume increase of approximately 3 pct (corresponding to a linear change of 1 pct) is associated with the austenite to martensite transformation. The transformation strains augment the ductility and add to the fracture toughness. The volumetric expansion tends to reduce the three dimensional tensile stresses that are developed during plastic straining near the apex of a notch. This changes the stress state toward a condition which favors a more ductile performance of a fracture toughness specimen.

At least in theory, steels with lower alloy content than TRIP steels, but with some TRIP characteristics, can be designed. The fracture toughness values for such steels should fall in the region between the maraging and the TRIP steel bands. (For additional details see references 56-58, 60, 69 and 70.)

## SUMMARY

The story of steel is inextricably entwined with the story of mankind. Whether it be peace or war, iron and steel have played a vital part in the evolution of society as we know it today. Progress in steel technology often coincided with the rise and fall of empires. The past two centuries have brought with them evolutionary and, at times, revolutionary changes in steelmaking.

The first significant advances in the understanding of the structure of solid metals and their alloys, i.e. physical metallurgy, came late in the history of metals and was largely associated with the burst of activity in the physical sciences during the last one hundred years. This period is now ending with the advent of a new era--an era which might appropriately be called "the era of alloy design", viz, the application of the first principles of materials science to the creation of new and superior engineering alloys. The era of alloy design was logically preceded by one in which the analytical and experimental tools, necessary for an atomistic understanding of solids, were developed and brought to high levels of sophistication.

The current state of development of alloy design, as seen from an academic viewpoint, is described with the aid of four illustrative examples taken from current student thesis research. These examples are: (1) a bcc Fe alloy having unusual toughness at temperatures of liquid nitrogen and below; (2) a series of medium alloy steels whose strength and toughness are equivalent to those of the high alloy maraging steels;

(3) the design of a bcc Fe alloy for elevated temperature service which utilizes intermetallic compounds rather than alloy carbides for dispersion hardening.

The "design" of the three alloys mentioned above was based on a mixture of basic science, engineering and empiricism. The significant fraction of empiricism remaining in current alloy design constitutes a formidable challenge to those who desire a completely rigorous approach to the creation of technologically useful materials. Judging from the past course of metals history, this challenge will be met.

#### ACKNOWLEDGMENTS

This research was performed under the auspices of the United States Atomic Energy Commission through the Inorganic Materials Research Division of the Lawrence Berkeley Laboratory. Additional support was also provided by the Army Materials and Mechanics Research Center.

REFERENCES

1. H. C. Sorby, J. Iron Steel Inst., (1886), 140
2. H. C. Sorby, J. Iron Steel Inst., (1887), 333.
3. W. Gibbs, Conn. Academy, 3 (1876), 152.
4. H. Jüptner von Jonstorff, Baumaterialienkunde, 2 (1897), 5.
5. H. Le Chatelier, Compt. rend., 130 (1900), 85.
6. B. Roozeboom, J. Iron Steel Inst., (1900), 311.
7. B. Roozeboom, Die Heterogenen Gleichgewichte, Braunschweig, 1901.
8. J. Groh and G. von Hevesy, Ann. Physik, 63 (1920), 85.
9. M. J. Stefan, Wien, Akad. Ber., 79 (1879), 161.
10. A. Fick, Pogg. Ann., (1855), 94.
11. G. Grube, Ztsch. Elektrochemie, 38 (1932), 797
12. C. Matano, Japanese J. Phys., 8 (1933), 109.
13. G. von Hevesy, Sitzber Akad. Wiss. Wein. Math.-Matr. Klasse, 11 A (1920), 129.
14. S. Dushman and I. Langmuir, Phys. Rev., 20 (1922), 113.
15. A. H. Cottrell, Dislocations and Plastic Flow in Crystals, Oxford University Press, Oxford, 1953.
16. J. Friedel, Dislocations, Pergamon Press, New York, 1964.
17. G. I. Taylor, Proc. Roy. Soc. (London), A 145 (1934), 362.
18. E. Orowan, Z. Physik, 89 (1934), 660.
19. J. M. Burgers, Proc. Kon. Ned. Akad. Wet., 42 (1939), 293
20. J. Washburn and E. R. Parker, Trans. Met Soc. Amer. Inst. Min. Met. Engrs. (1952), 1076.

21. M. J. Whelan, P. B. Hirsch, R. W. Horne, and W. Bollmann, Proc. Roy. Soc., A 240 (1957), 524.
22. E. S. Davenport and E. C. Bain, Trans. Met. Soc. Amer. Inst. Min. Met. Engrs., (1930), 117.
23. E. C. Bain, Trans. Amer. Soc. Metals, 20 (1932), 385.
24. Atlas of Isothermal Transformation Diagrams, United States Steel Corporation, Pittsburgh, Pa., 3rd edition, 1963.
25. F. R. Schwartzberg, S. H. Osgood, R. D. Keys, and T. I. Kiefer, Cryogenic Materials Data Handbook, Technical Documentary Report No. ML-TDR-64-280, Martin Co., Denver, Colorado, 1964.
26. W. A. Horwood, M. S. Thesis, LBL-1121, University of California, Berkeley, California, December 1972.
27. S. Jin, W. A. Horwood, J. W. Morris, Jr., and V. F. Zackay, Advan. Cryog. Eng., in press.
28. S. Jin, J. W. Morris, Jr., and V. F. Zackay, Advan. Cryog. Eng., in press.
29. G. Sasaki, D. Eng. Thesis, LBL-1493, University of California, Berkeley, California, July 1973.
30. V. F. Zackay, Microstructure and Design of Alloys, Institute of Metals, London, 1973, p. 591.
31. S. Jin, J. W. Morris, Jr., and V. F. Zackay, presented at Materials Engineering Congress, Chicago, Illinois, October 1973.
32. R. W. Guard, Mechanical Behavior of Materials at Elevated Temperature, J. E. Dorn, ed., McGraw-Hill Book Co., Inc., New York, 1961, p. 270.
33. L. H. Toft and R. A. Marsden, Special Report No. 70, The Iron and Steel Institute, London, 1961, p. 276.

34. J. R. Mihalisin, C. G. Bieber, and R. T. Grant, Trans. Met. Soc. Amer. Inst. Min. Met. Engrs., 242 (1968), 2399.
35. R. F. Decker, Steel-Strengthening Mechanisms, symposium sponsored by Climax Molybdenum Co., 1969, p. 147.
36. R. H. Jones, E. R. Parker, and V. F. Zackay, Proc. Fifth Intern. Mater. Symposium, Berkeley, California, September 1971, p. 829.
37. M. Hansen, Constitution of Binary Alloys, 2nd edition, McGraw-Hill Book Co., Inc., New York, 1958, p. 525.
38. G. A. Mellor and S. M. Barker, J. Iron Steel Inst., 194 (1960), 464.
39. J. H. Woodhead and A. G. Quarrell, J. Iron Steel Inst., 203 (1965), 605.
40. A. K. Sinha and W. Hume-Rothery, J. Iron Steel Inst., 205 (1967), 671.
41. S. Jin, M. S. Thesis, LBL-443, University of California, Berkeley, California, December 1971.
42. D. Bhandarkar, D. Eng. Thesis, LBL-1858, University of California, Berkeley, California, September 1973.
43. Metals Handbook, Vol. 1, 8th ed., American Society for Metals, Metals Park, Ohio, 1969.
44. C. R. Austin, C. R. St. John, and R. W. Lindsay, Trans. Met. Soc. Amer. Inst. Min. Met. Engrs., 162 (1945), 84.
45. S. F. Reiter and W. R. Hibbard, Jr., Trans. Met. Soc. Amer. Inst. Min. Met. Engrs., 203 (1955), 655.
46. E. R. Parker, Proc. Amer. Soc. Testing Mater., 60 (1960), 1.

47. V. F. Zackay, E. R. Parker, and D. Bhandarkar, Proc. John E. Dorn Memorial Symposium on Rate Processes in Plastic Deformation, Cleveland, Ohio, October 1972. Also LBL-1174, Lawrence Berkeley Laboratory, Berkeley, California, October 1972.
48. M. S. Bhat, M. S. Thesis, University of California, Berkeley, California, unpublished.
49. D. Bhandarkar, M. S. Bhat, V. F. Zackay, and E. R. Parker, unpublished.
50. S. J. Matas, Metals Eng. Q., 4 (1964), 48.
51. C. L. M. Cottrell, Fracture Toughness of High Strength Materials: Theory and Practice, ISI Publication 120, The Iron and Steel Institute, London, 1970, p. 112.
52. D. Huang and G. Thomas, Met. Trans., 2 (1971), 1587.
53. D. Huang and G. Thomas, Met. Trans., 3 (1972), 343.
54. G. Thomas, Iron Steel Intern., 1973, in press. Also LBL-1871, Lawrence Berkeley Laboratory, Berkeley, California.
55. E. A. Steigerwald, Metal Progr., 92 (1967), 97.
56. V. F. Zackay, E. R. Parker, R. D. Goolsby, and W. E. Wood, Nature Phys. Sci., 236 (1972), 108.
57. E. R. Parker and V. F. Zackay, Eng. Fr. Mech., 5 (1973), 147.
58. V. F. Zackay, E. R. Parker, and W. E. Wood, Microstructure and Design of Alloys, Institute of Metals, London, 1973, p. 175.
59. Annual Book of ASTM Standards, Part 31, American Society for Testing Materials, Philadelphia, 1972, p. 955.

60. W. E. Wood, E. R. Parker, and V. F. Zackay, LBL-1474, Lawrence Berkeley Laboratory, University of California, Berkeley, California, May 1973.
61. A. Seal and R. W. K. Honeycombe, J. Iron Steel Inst., 188 (1958), 9.
62. D. Webster, Met. Trans., 2 (1971), 2097.
63. M. Tanaka and J. Yamamoto, Toward Improved Ductility and Toughness, Climax Molybdenum Development Co. (Japan) Ltd., 1971, p. 195.
64. J. A. McMahon and G. Thomas, Microstructure and Design of Alloys, Institute of Metals, London, 1973, p. 180.
65. W. W. Gerberich, P. L. Hemmings, M. D. Merz, and V. F. Zackay, Trans. Amer. Soc. Metals, 61 (1968), 843.
66. W. W. Gerberich, P. L. Hemmings, V. F. Zackay, and E. R. Parker, Fracture 1969, P. L. Pratt, ed., Chapman and Hall Ltd., London, 1969, p. 288.
67. S. D. Antolovich and B. Singh, Met. Trans. 2 (1971), 2135.
68. W. W. Gerberich, P. L. Hemmings, and V. F. Zackay, Met. Trans., 2 (1971), 2243.
69. G. Lai, W. E. Wood, E. R. Parker, and V. F. Zackay, unpublished.
70. T. Tom, D. Eng. Thesis, LBL-1856, University of California, Berkeley, California, September 1973.



FIGURE CAPTIONS

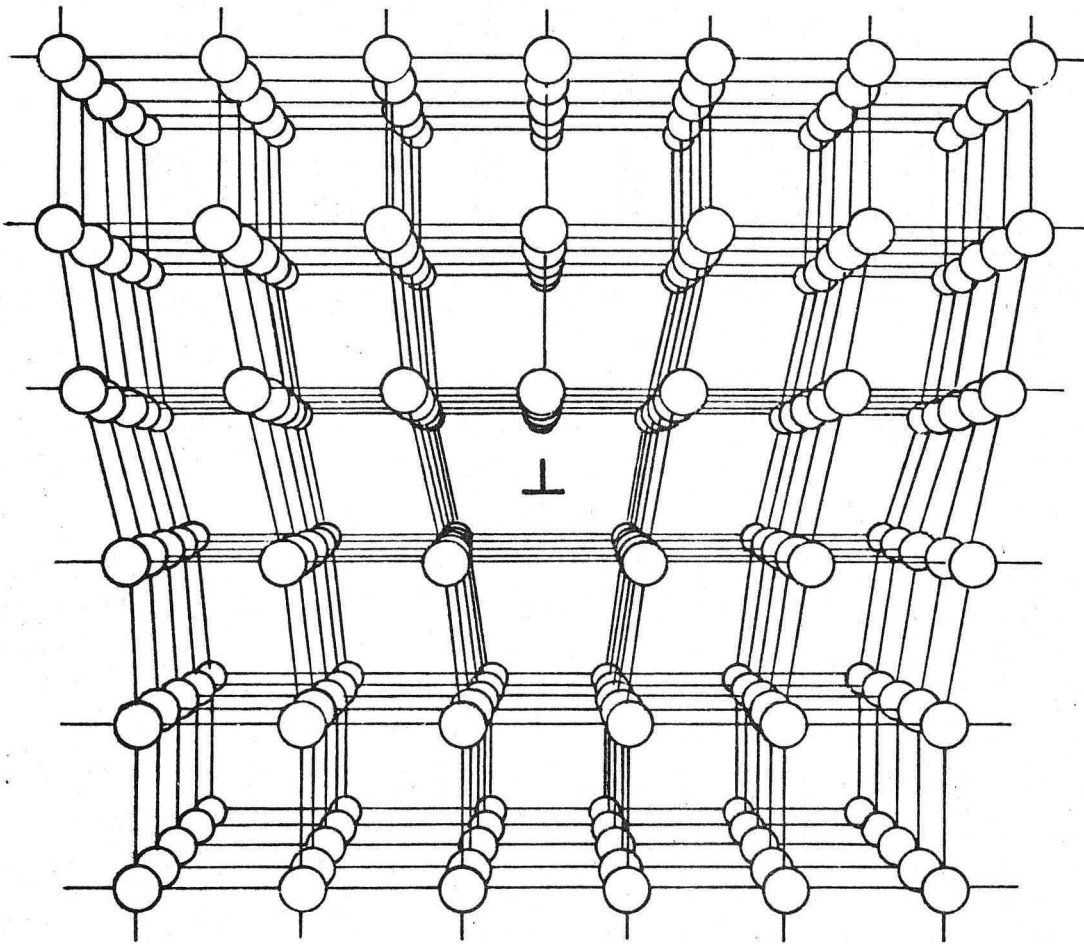
- Fig. 1 Three-dimensional sketch illustrating the nature of the crystal defect called an edge dislocation.
- Fig. 2 Photograph of a screw dislocation model. The model has been sheared on one side of the defect, but not on the other. There are no missing atoms in this type of dislocation.
- Fig. 3 Sketch of an edge dislocation showing that atoms move distances that are smaller than the atom spacing as the defect is moved a complete spacing. The open circles show atom positions before the dislocation has moved, and the filled circles are the positions after movement.
- Fig. 4 Photograph of a zinc single crystal that has been plastically deformed by a load applied along its cylindrical axis. Plastic flow occurred by movement of dislocations along randomly spaced planes of atoms, producing slip offsets.
- Fig. 5 Photomicrograph of quenched steel that has been reheated. The carbide particles are nearly spherical in shape.
- Fig. 6. Graph showing how the room temperature yield strength of a quenched steel becomes lower as the reheating temperature is increased.
- Fig. 7 Photomicrograph showing the plate-like structure of  $\text{Fe}_3\text{C}$  that forms in slowly cooled steel.
- Fig. 8 Diagram for a 0.8 pct steel showing time required for austenite to transform isothermally when quenched from the stable austenite range to lower temperatures (adapted from ref. 24).

- Fig. 9 Diagram for an alloy steel, AISI 4340 (containing 1.75 pct Ni, 0.80 pct Cr, 0.25 pct Mo, 0.40 pct C), showing time required for austenite to transform isothermally when quenched from the stable austenite range to lower temperatures (adapted from ref. 24).
- Fig. 10 Diagram for AISI 4340 steel determined by the more sensitive magnetic method, which is capable of resolving the short time portions of the overlapping upper bainite and lower bainite curves.
- Fig. 11 The effect of reheat temperature on (a) the grain size of the Fe-12Ni-0.5Ti alloy, and (b) the Charpy V-notch impact energy at  $-196^{\circ}\text{C}$  for the Fe-12Ni-0.5Ti and Fe-12Ni-0.25Ti alloys. The time at reheat temperature was 2 hr in each case.
- Fig. 12 Macrographs of broken Charpy bars, optical micrographs of microstructure, and scanning electron fractographs of Charpy bars of the Fe-12-Ni-0.5Ti alloy reheated for 2 hr at the indicated temperatures, tested at  $-196^{\circ}\text{C}$ .
- Fig. 13 The effect of time of reheat at indicated temperatures on the Charpy V-notch impact energy at  $-196^{\circ}\text{C}$  for the Fe-12Ni-0.5Ti alloy. The grain size in microns is shown in parentheses on the curves.
- Fig. 14 A comparative plot of the yield strength and Charpy V-notch impact toughness, both measured at  $-196^{\circ}\text{C}$ , for two commercial cryogenic steels<sup>24</sup> and the Fe-12Ni-0.5Ti alloy.
- Fig. 15 Iron-rich portion of the equilibrium phase diagram of the Fe-Ta system.

- Fig. 16 Optical micrographs showing the microstructure of alloy Ta7Cr, (a) aged at 700°C for 40 min, and (b) aged at 700°C, and spheroidized at 1100°C for 10 min.
- Fig. 17 Transmission electron micrograph of a carbon replica showing the Laves phase particles extracted from alloy Ta7Cr spheroidized at 1100°C for 10 min.
- Fig. 18 Scanning electron fractographs of alloy Ta7Cr tested in tensile tests at 22°C following (a) aging at 700°C for 40 min, and (b) aging at 700°C, and spheroidizing at 1100°C for 10 min.
- Fig. 19 Effect of test temperature on the short time yield strength, ultimate tensile strength, and fracture elongation of spheroidized alloy Ta7Cr.
- Fig. 20 Stress vs rupture time at 1100°F (593°C) for alloys Ta7Cr and Ta7CrMo. Also shown are the results reported in the literature<sup>54</sup> for 0.3C-1Cr-1Mo-0.25V steel, 0.15C-9Cr-1Mo steel, Greek Ascoloy, and the AISI types 403, 410 and 422 stainless steels.
- Fig. 21 Influence of austenitizing temperature on the room temperature plane strain fracture toughness,  $K_{IC}$ , of as quenched 5Mo-0.3C steel.
- Fig. 22 Transmission electron micrographs of AISI 4340 steel heated to 1200°C before oil quenching, (a) bright field image, (b) dark field image, showing reversal of contrast at austenite films between martensite laths.

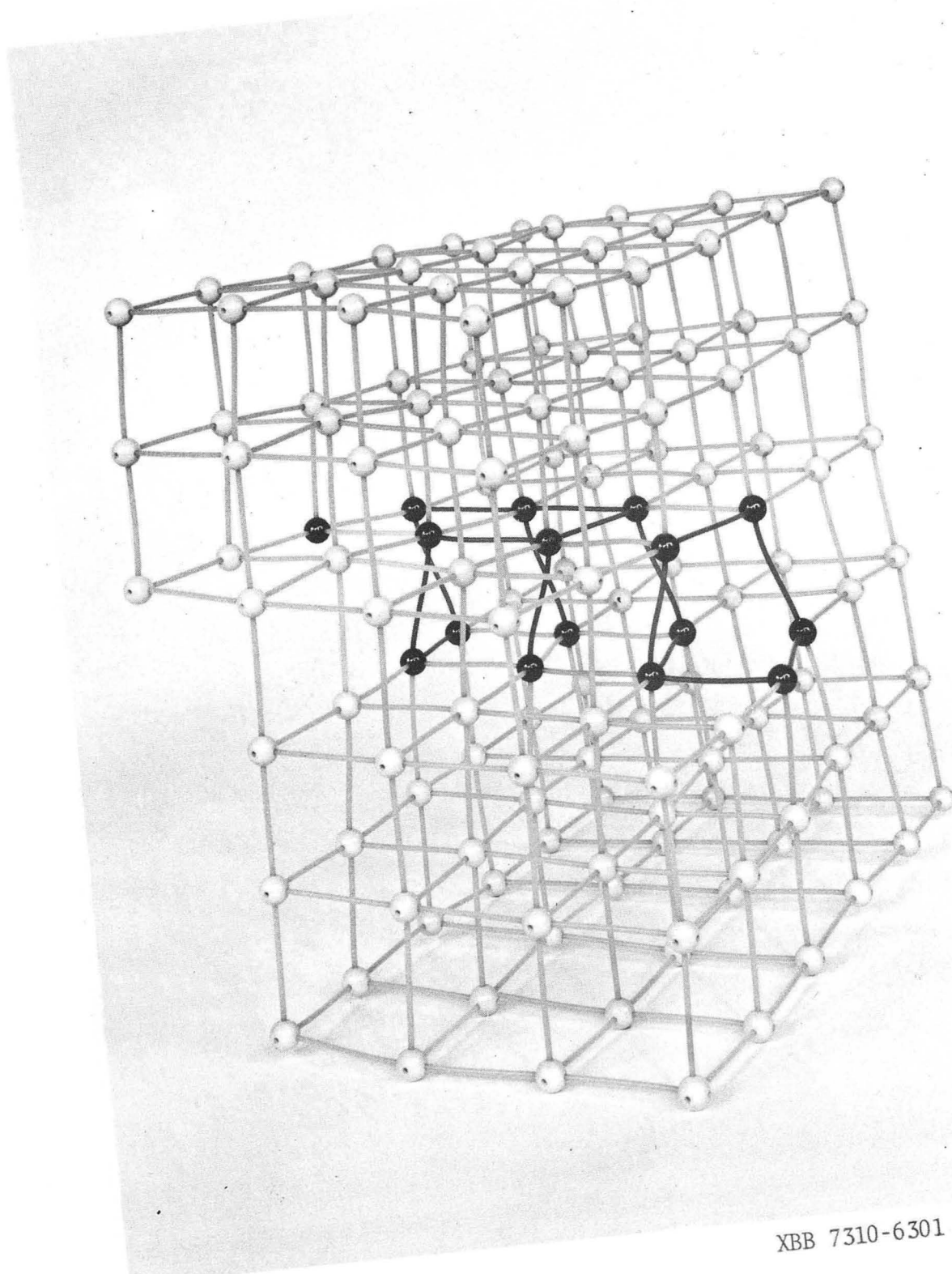
Fig. 23 Plots of fracture toughness,  $K_{IC}$ , vs yield strength. The two shaded bands represent the range of values found in the literature for AISI 4340 and maraging steels. The circles are data points from the present investigation.

Fig. 24 Plots of fracture toughness vs yield strength. Bands for commercial steels ( $K_{IC}$ ) and metastable austenitic TRIP steels ( $K_C$ ).



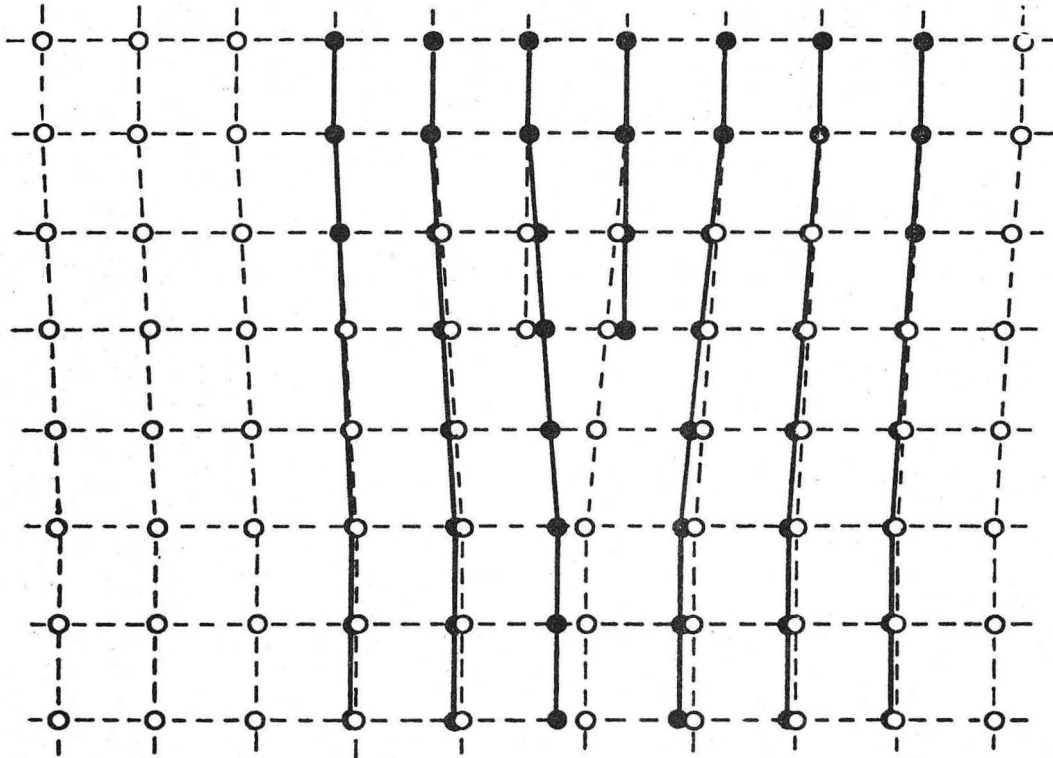
XBL7310-5493

Fig. 1



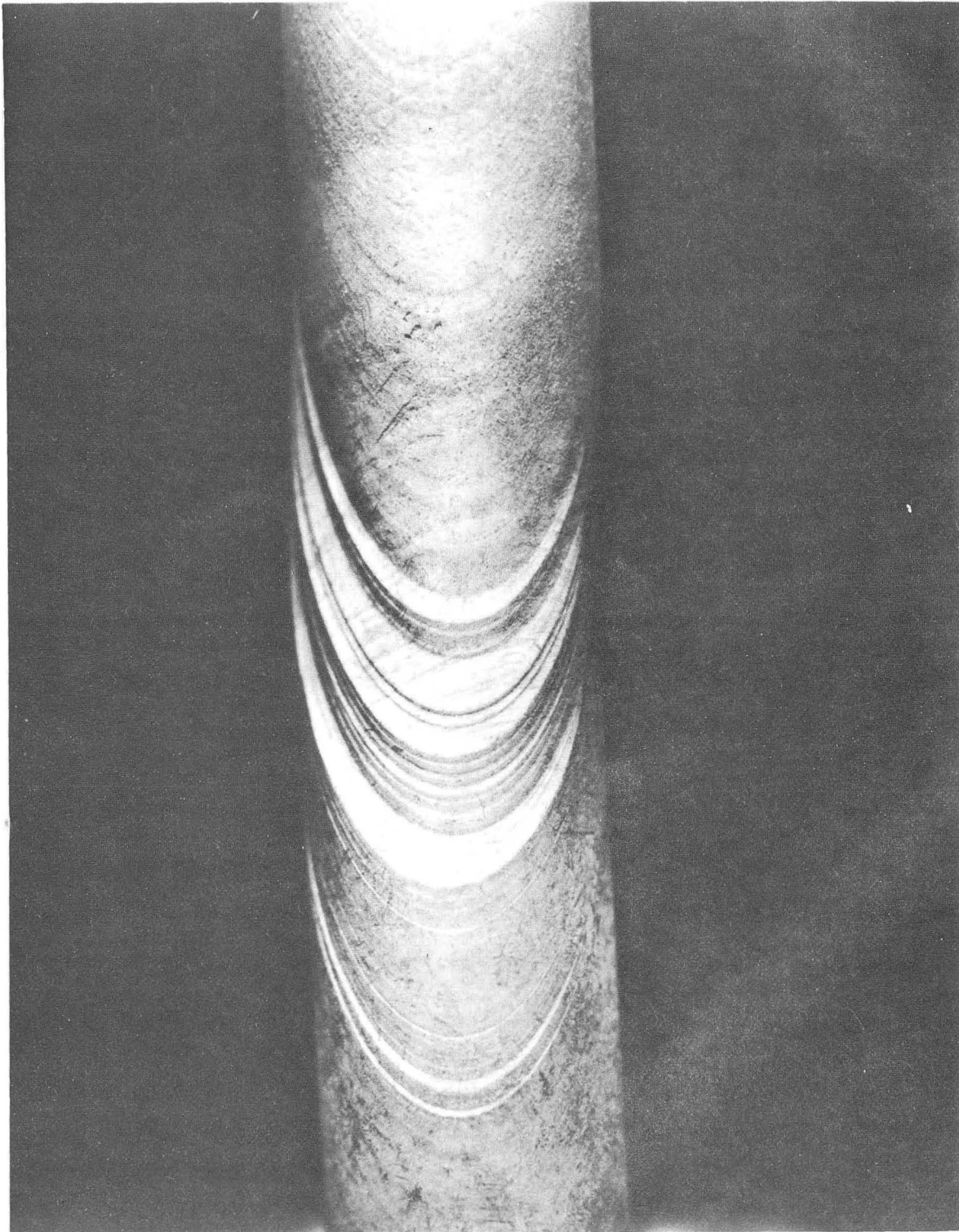
XBB 7310-6301

Fig. 2



XBL 7310-5492

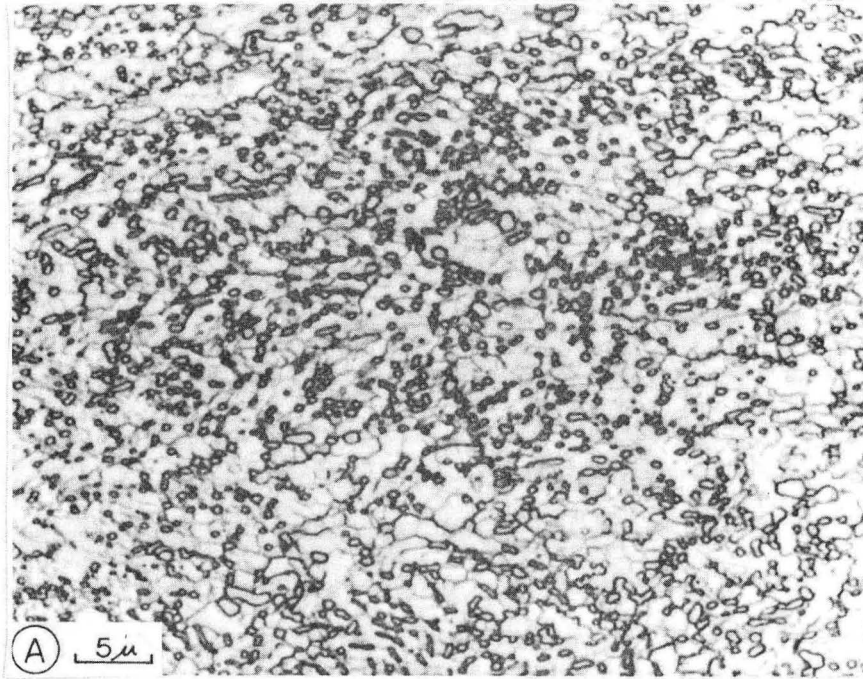
Fig. 3



XBB 7310-6254

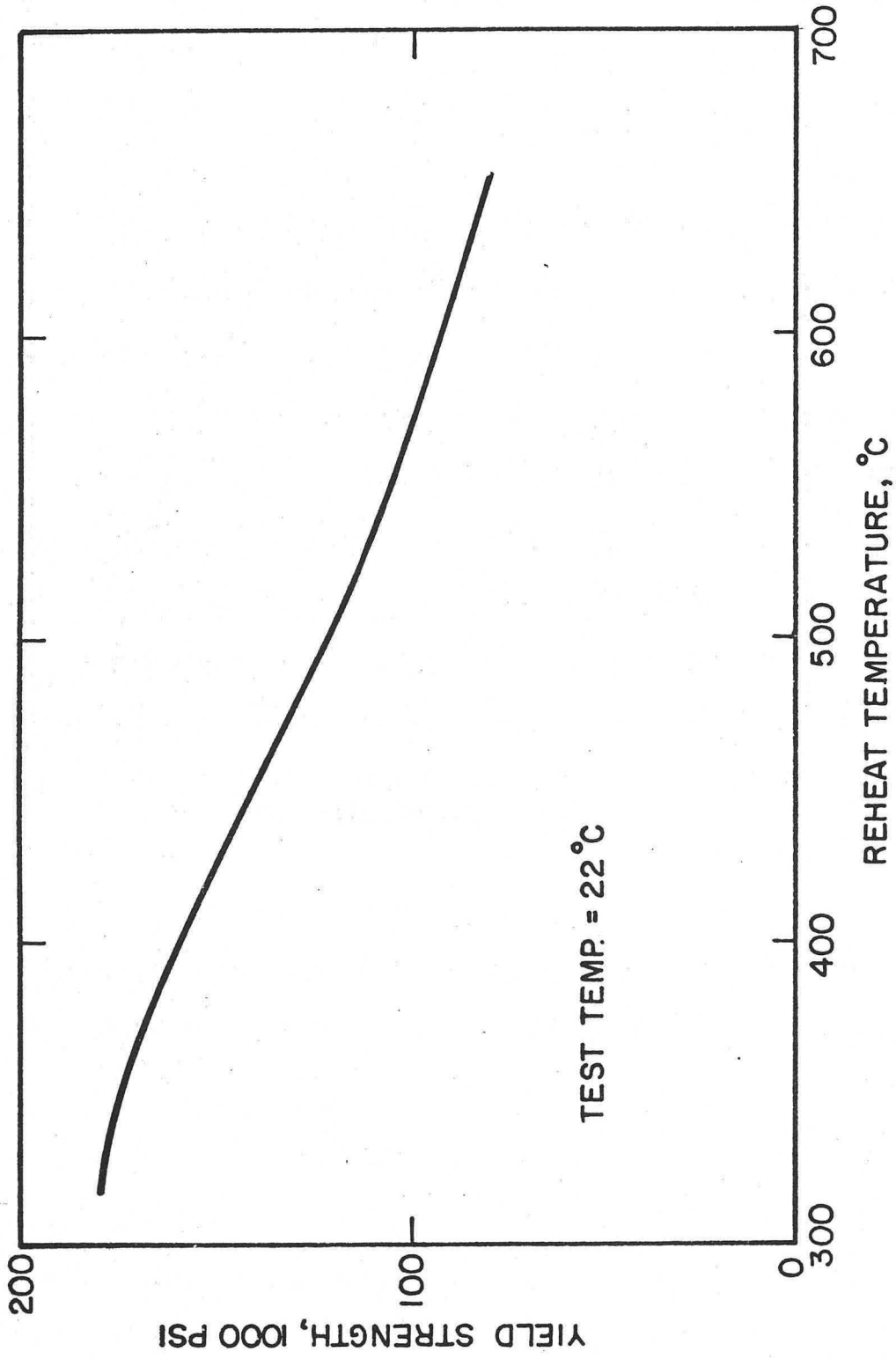
Fig. 4





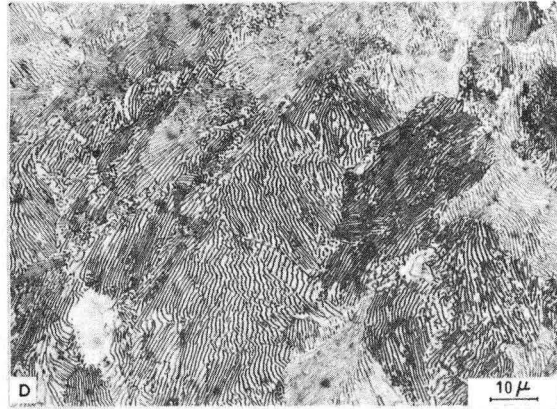
XBB 713-919 (A only)

Fig. 5



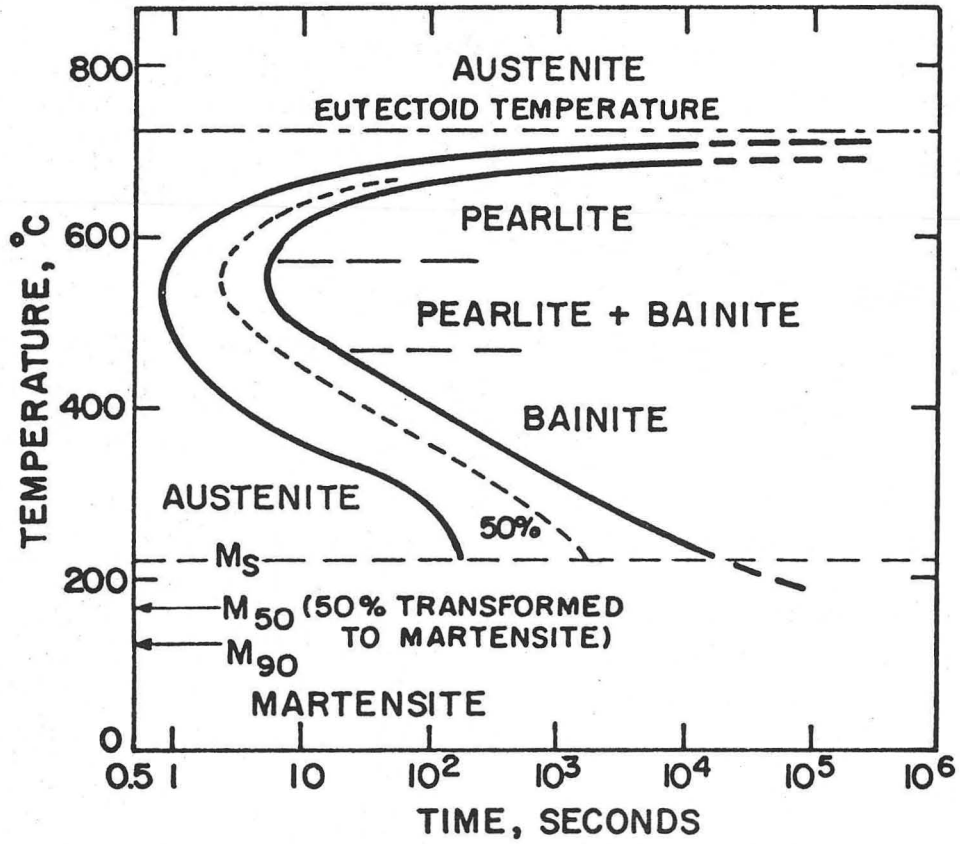
XBL 7310-549I

Fig. 6



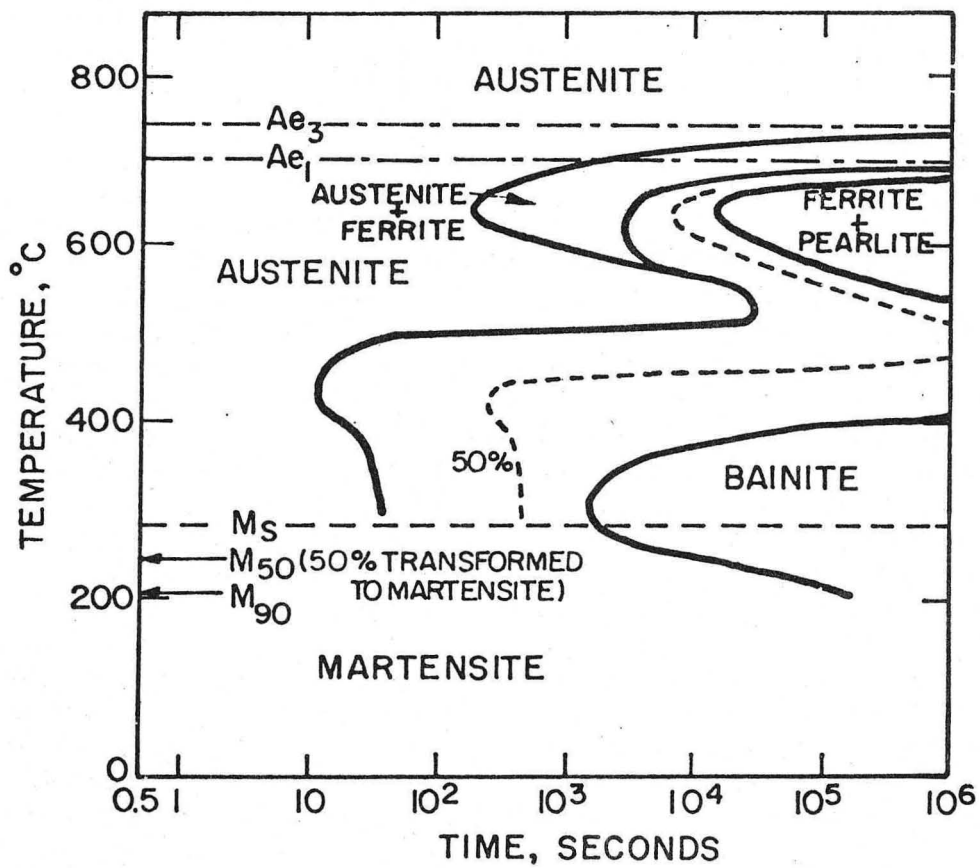
XBB 6910-6358  
(D only)

Fig. 7



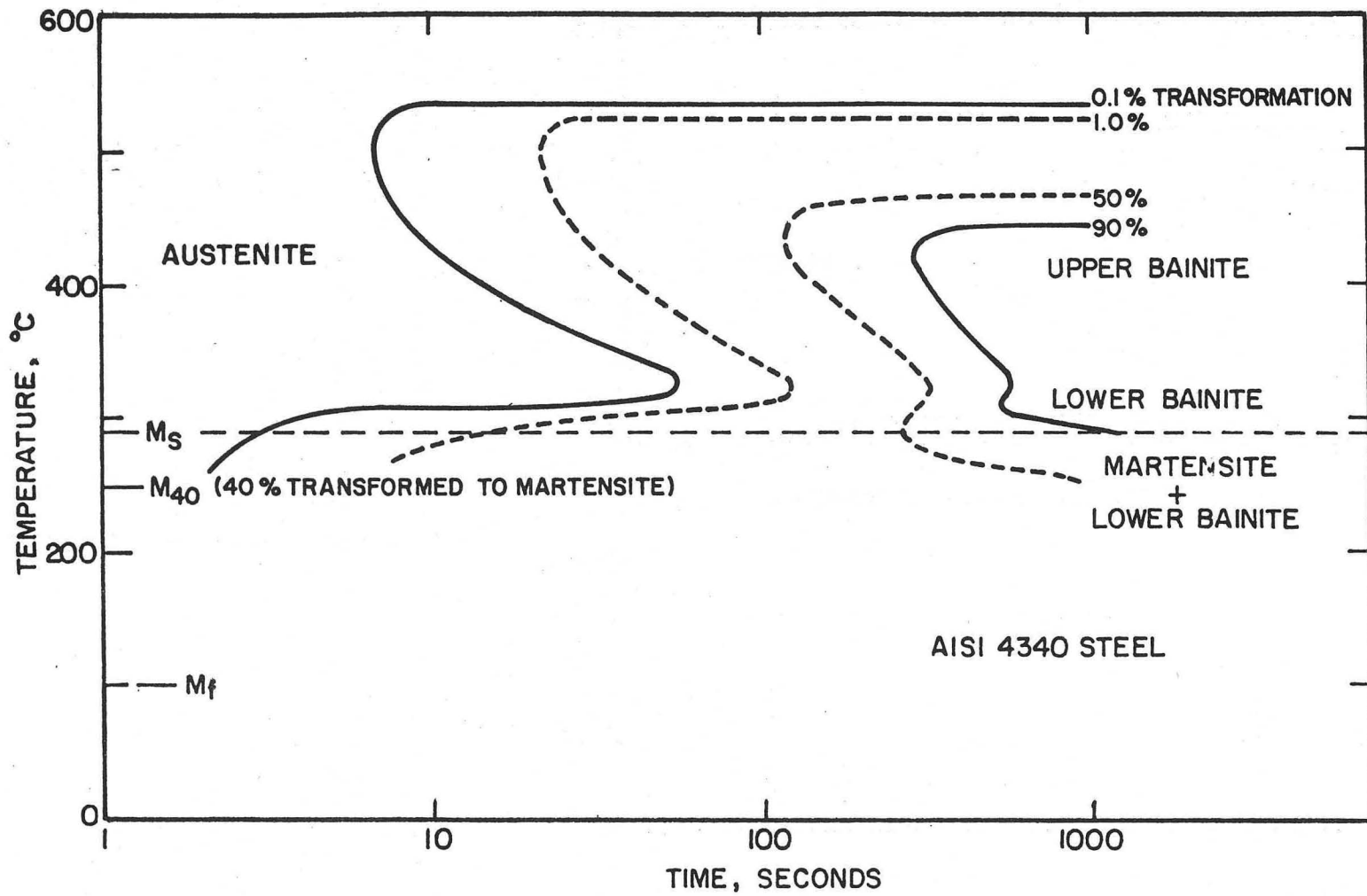
XBL7310-5488

Fig. 8



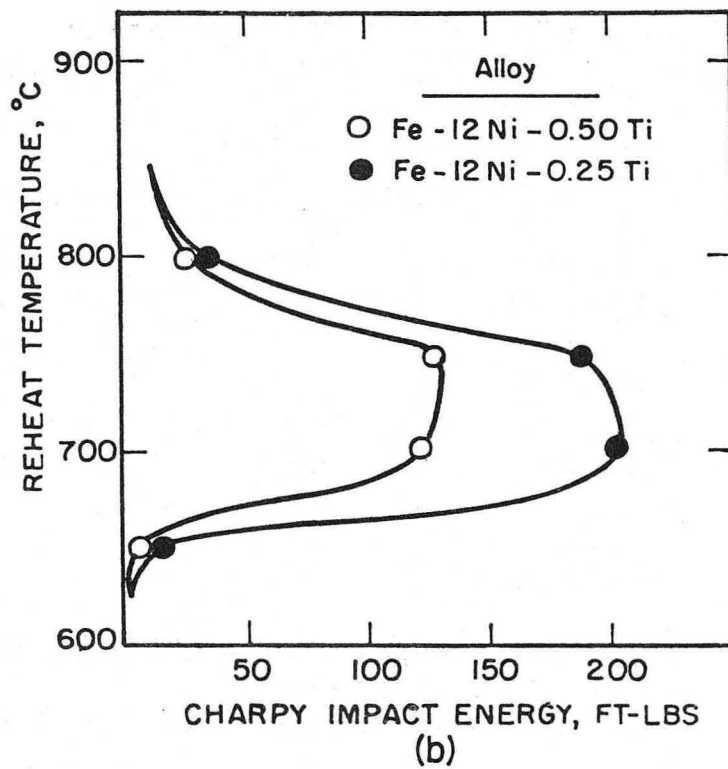
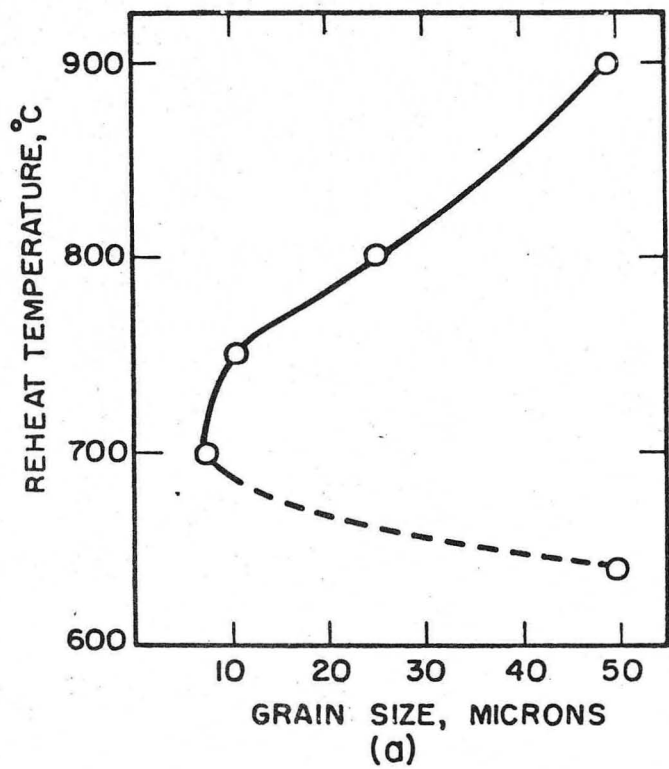
XBL7310-5489

Fig. 9



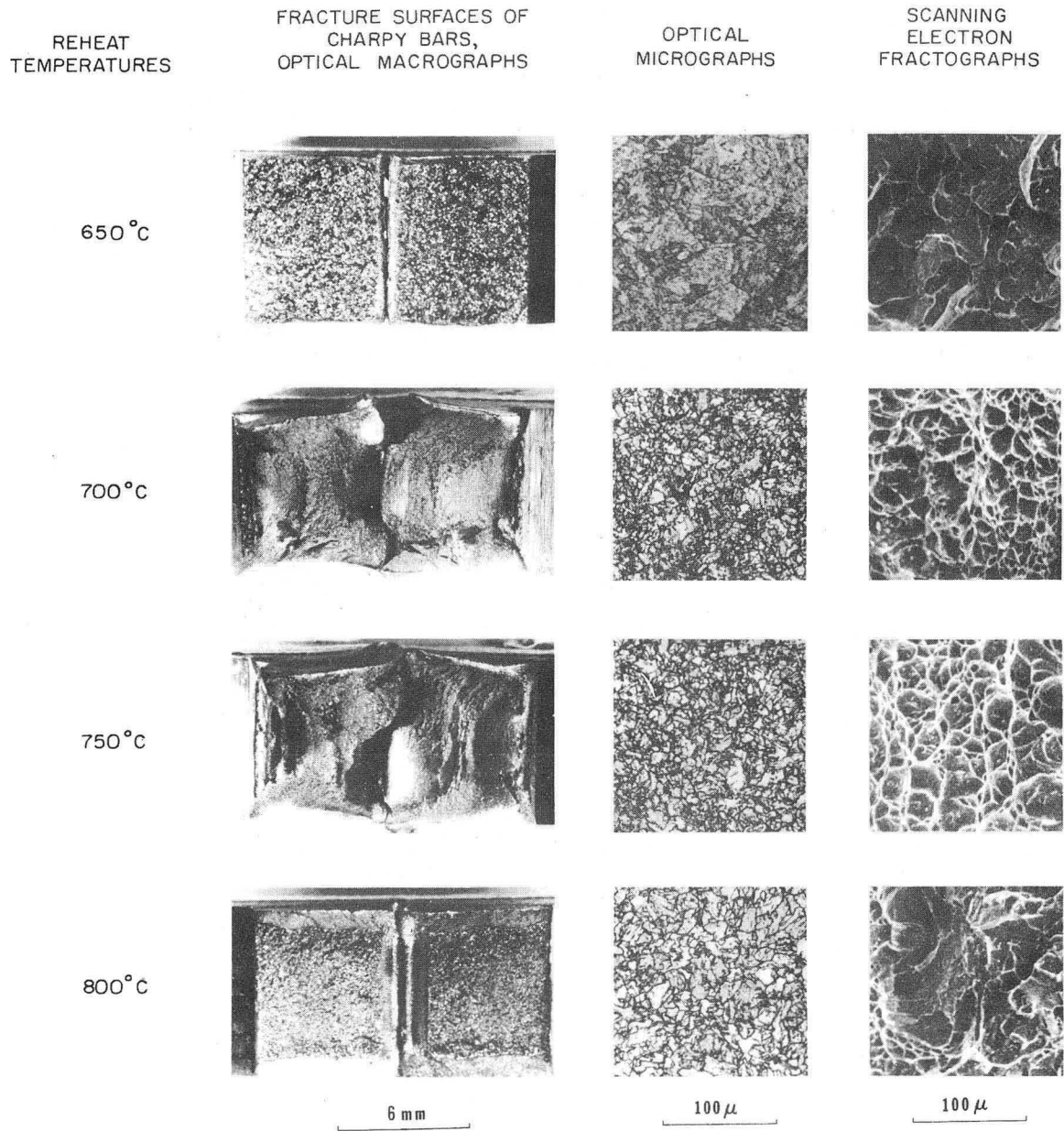
XBL 7310-5490

Fig. 10



XBL 733-5837

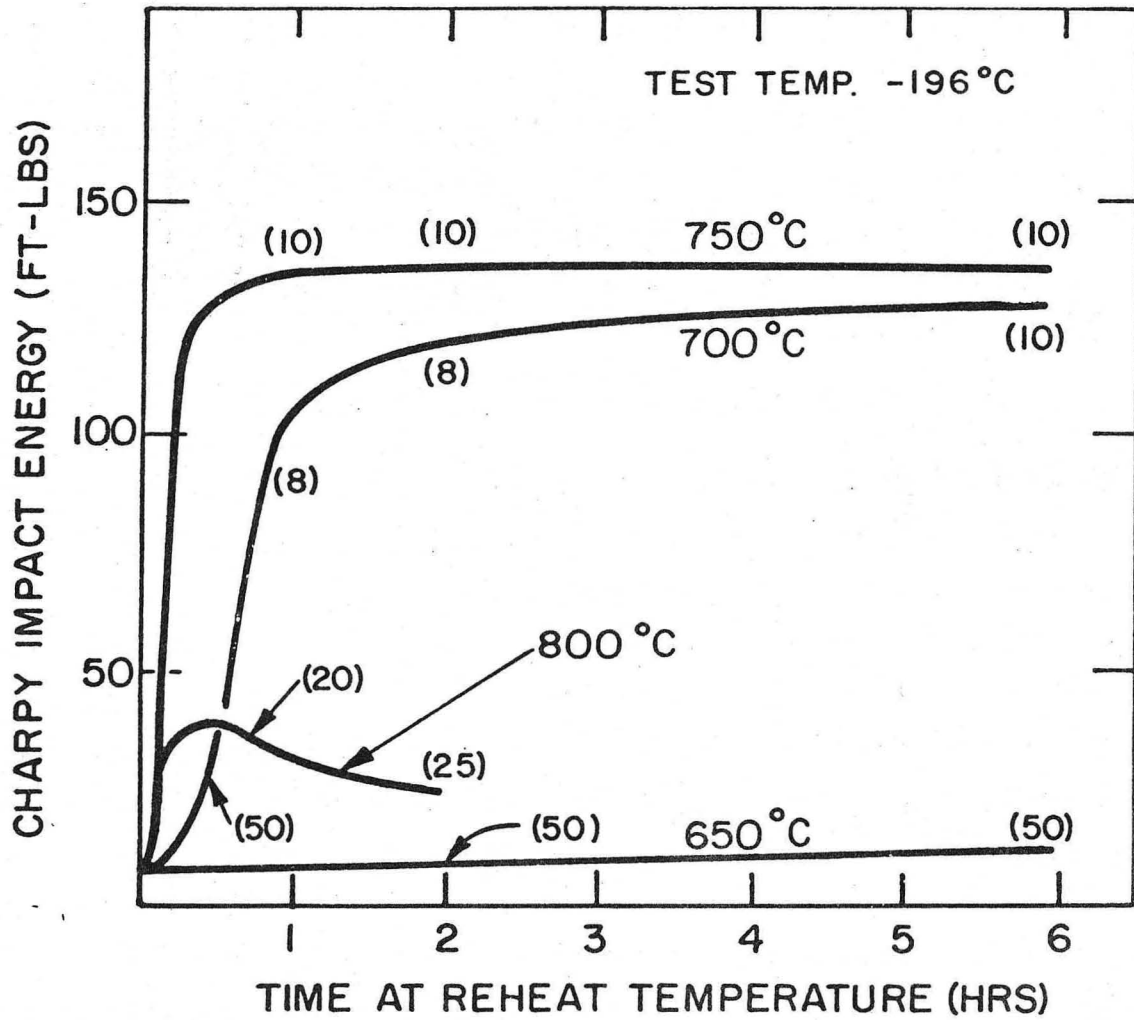
Fig. 11



XBB 733-1776

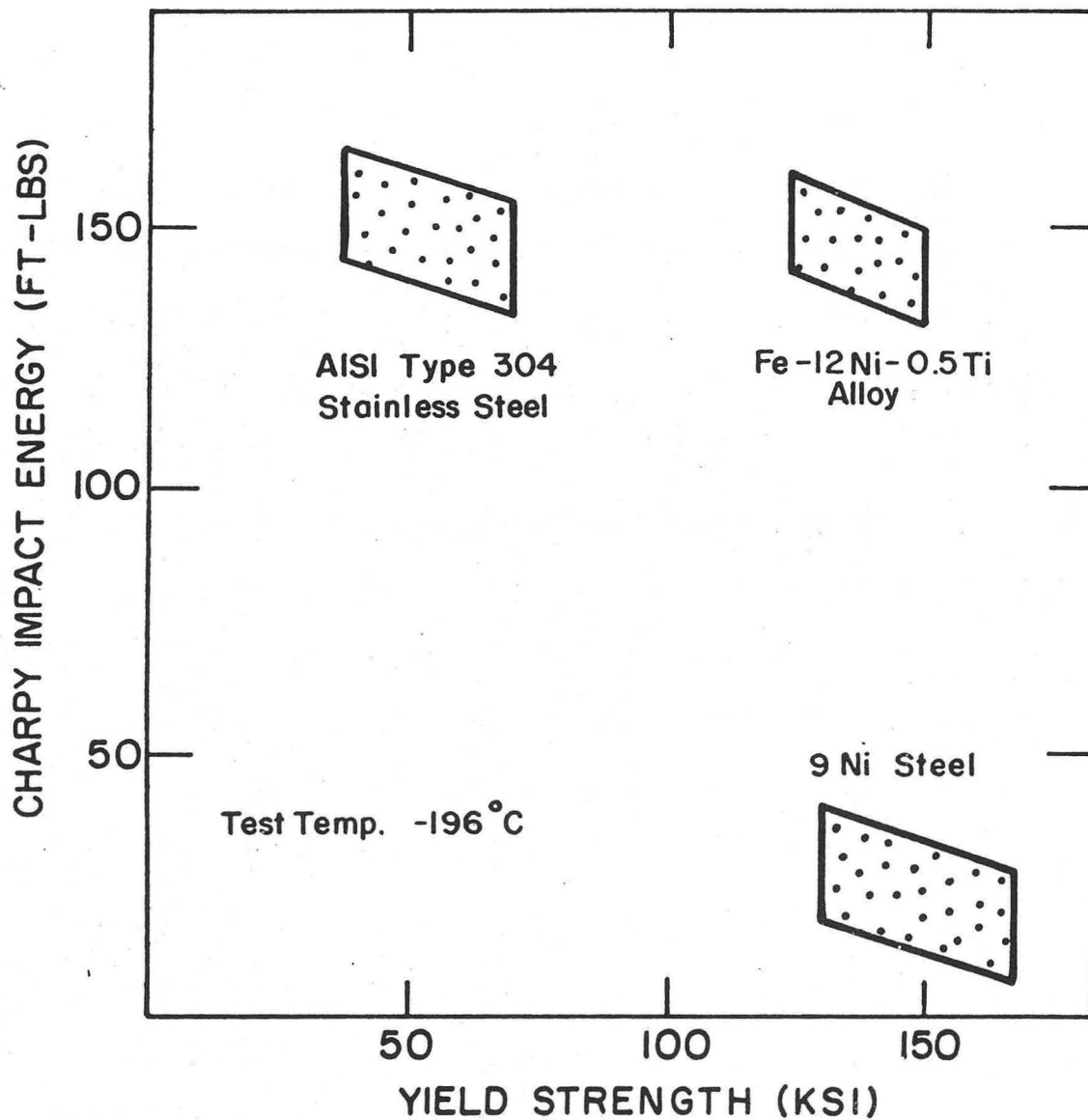
Fig. 12





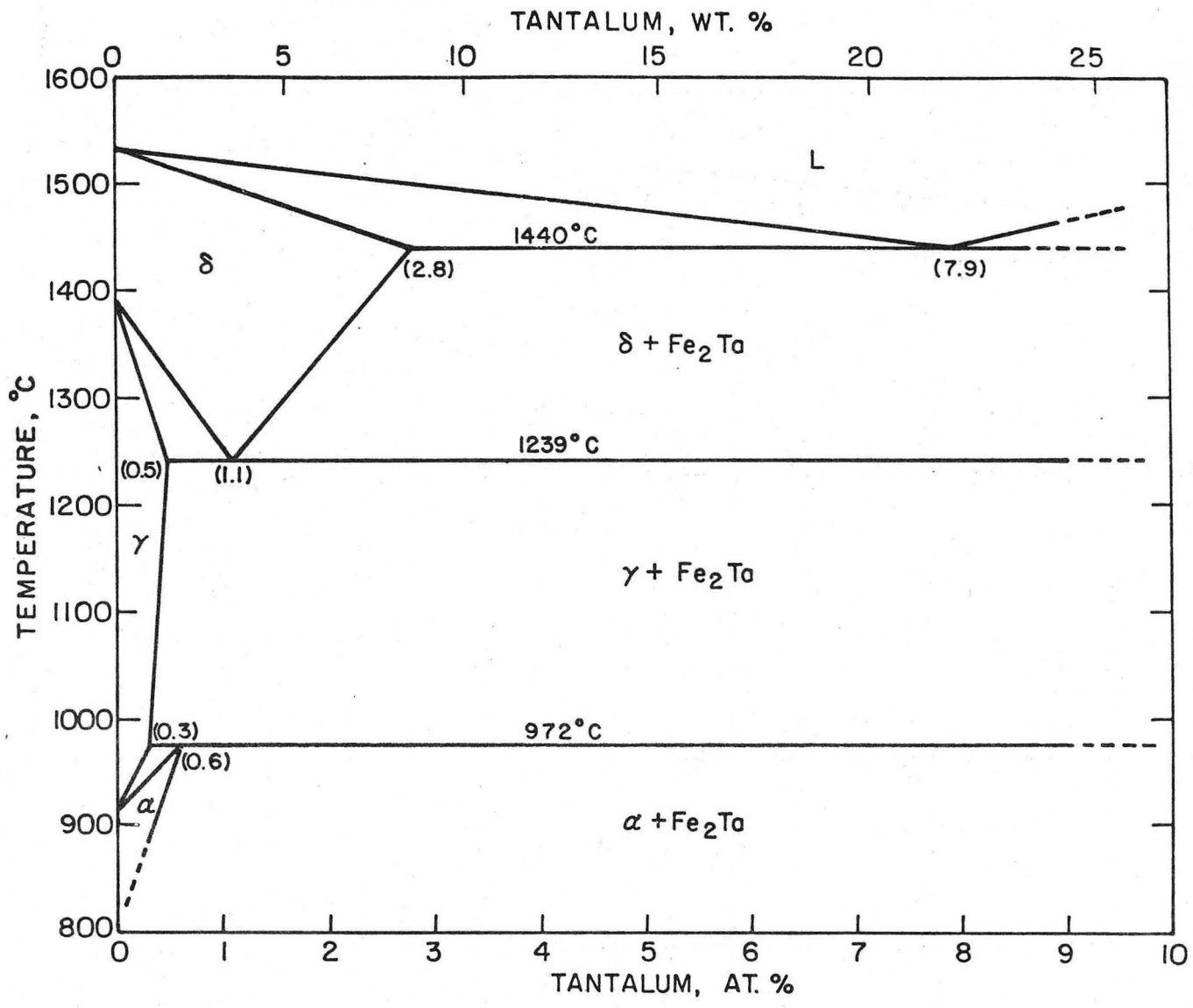
XBL 733 5836D

Fig. 13



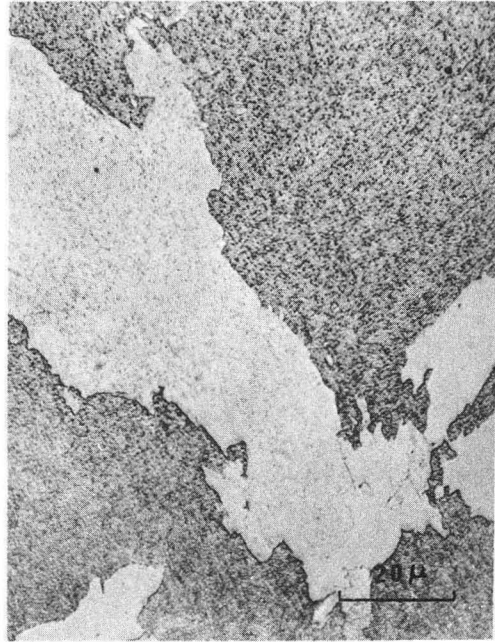
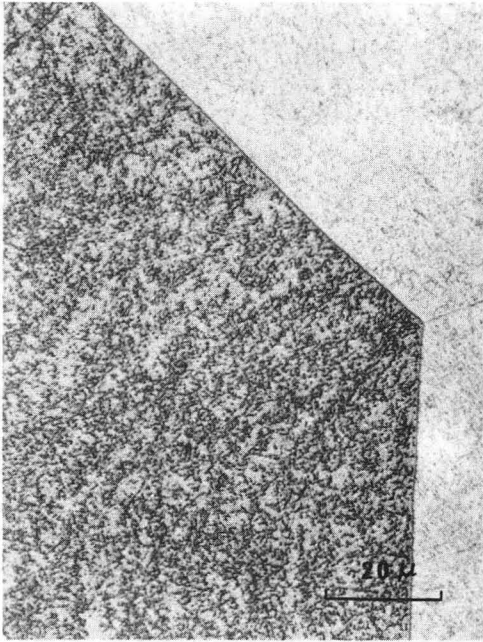
XBL 733-5836C

Fig. 14



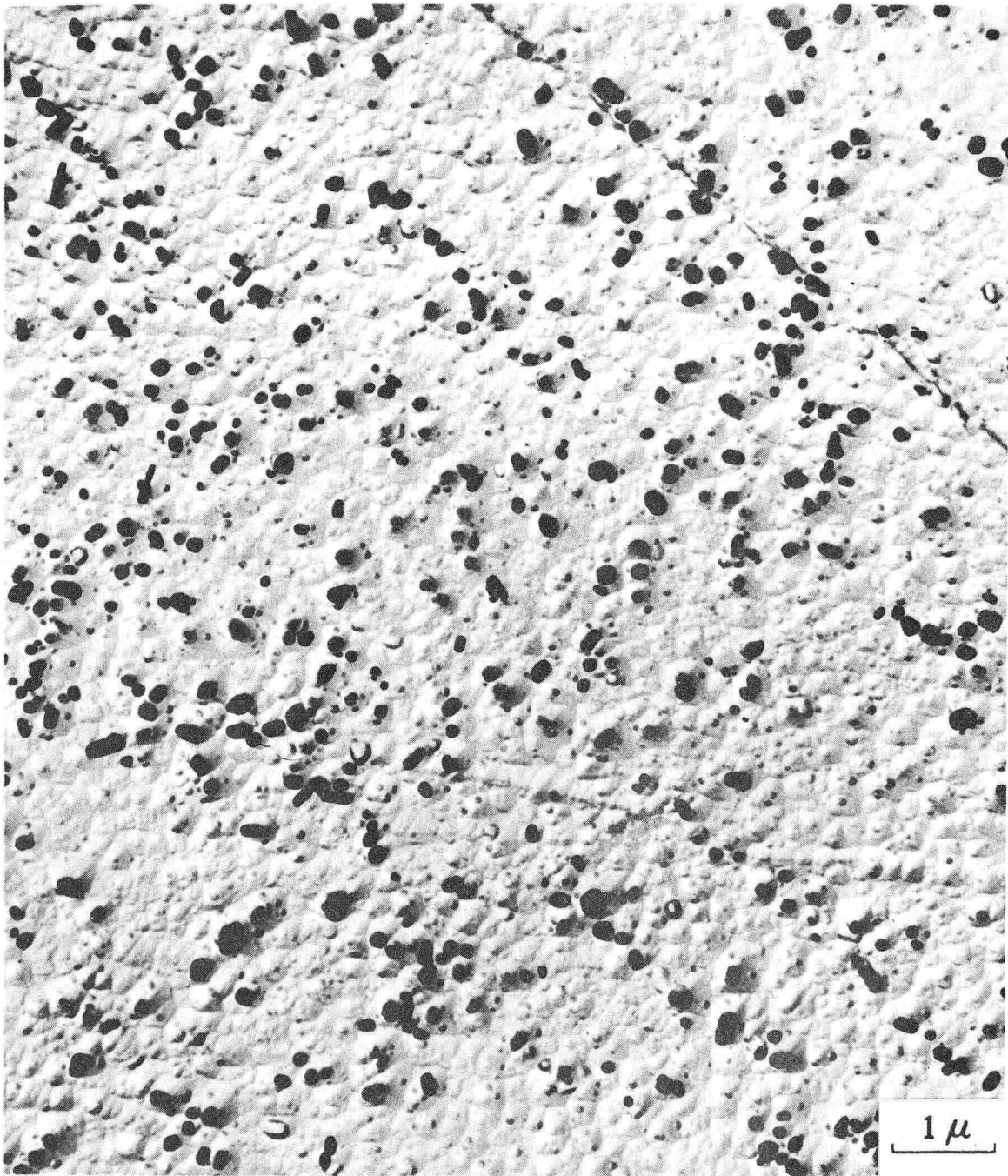
XBL721-5996

Fig. 15



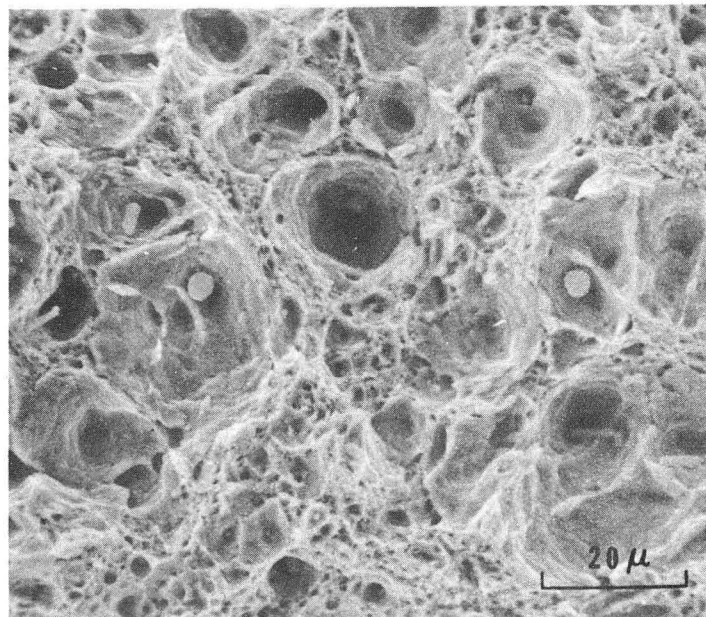
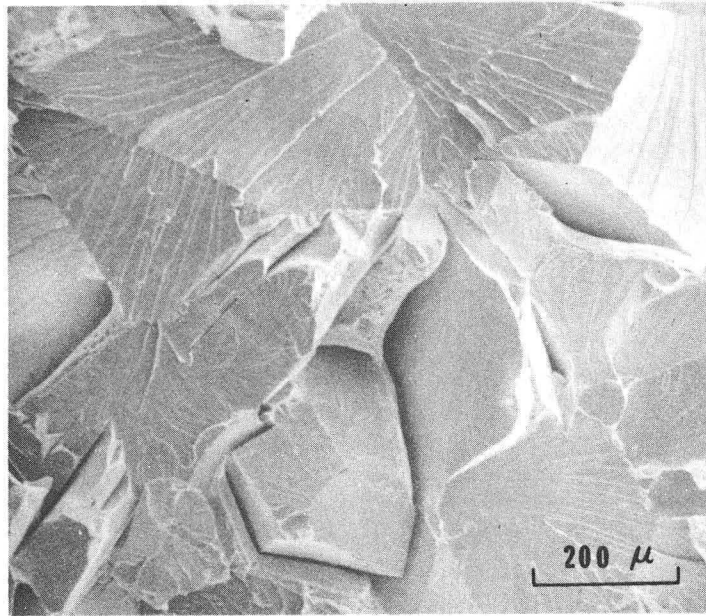
XBB 7210-4984

Fig. 16



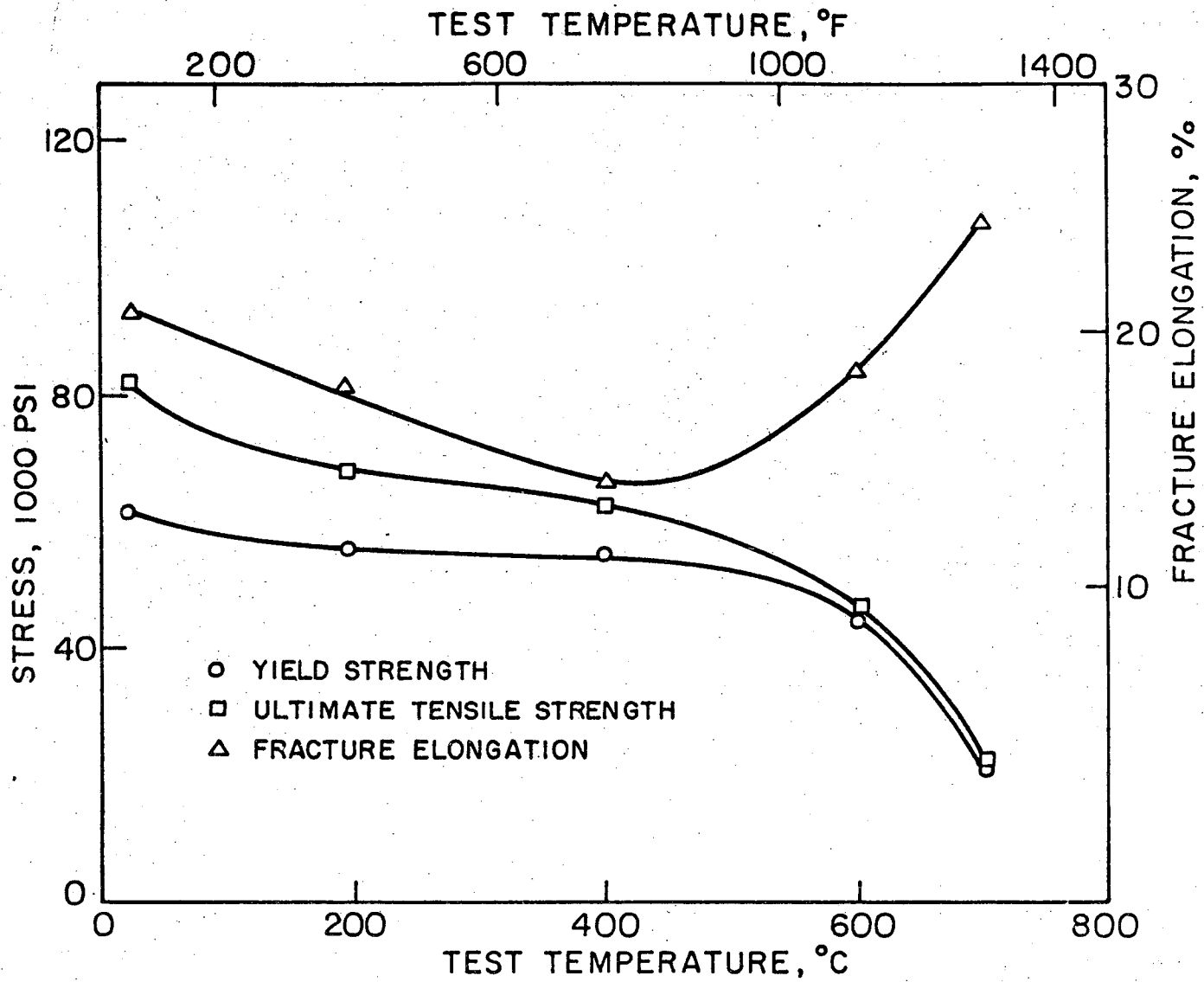
XBB 738-5043

Fig. 17



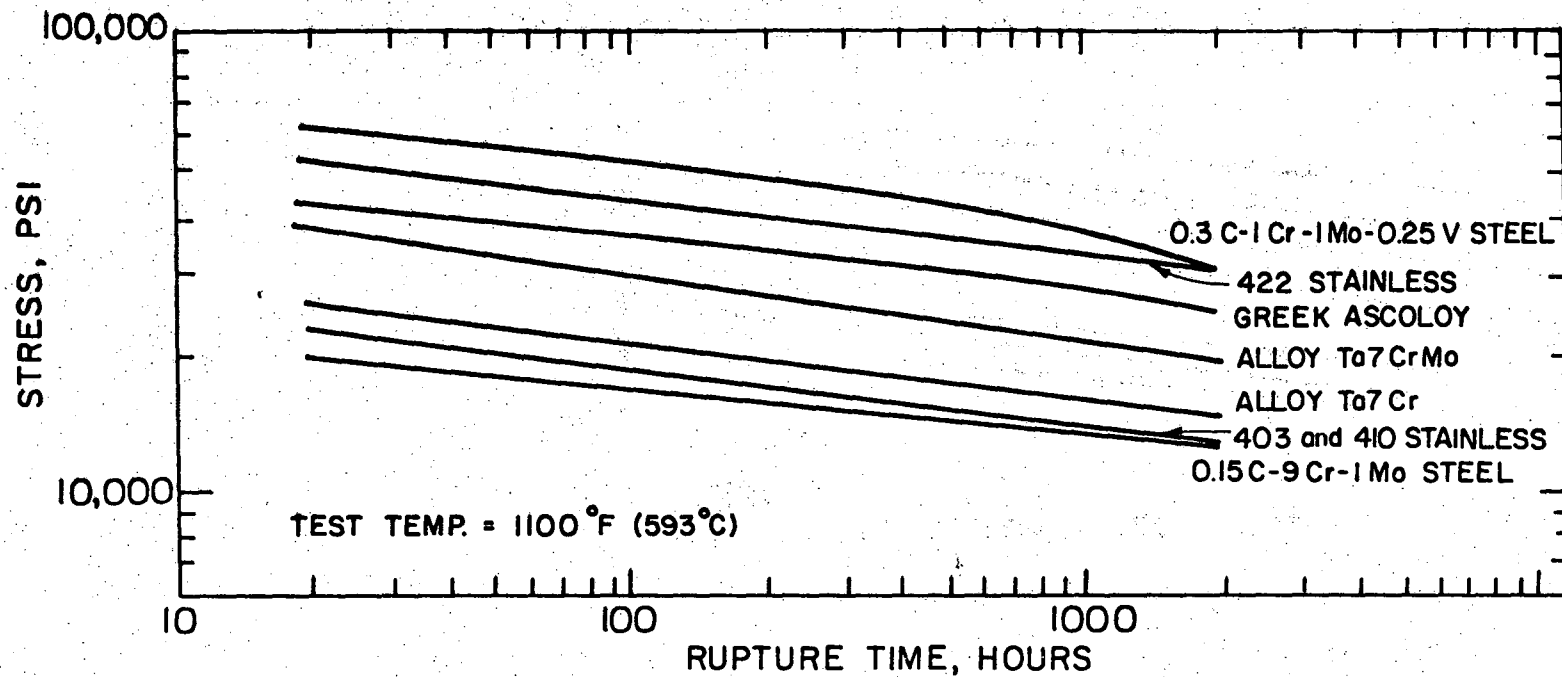
XBB 738-5037A

Fig. 18



XBL737-6449

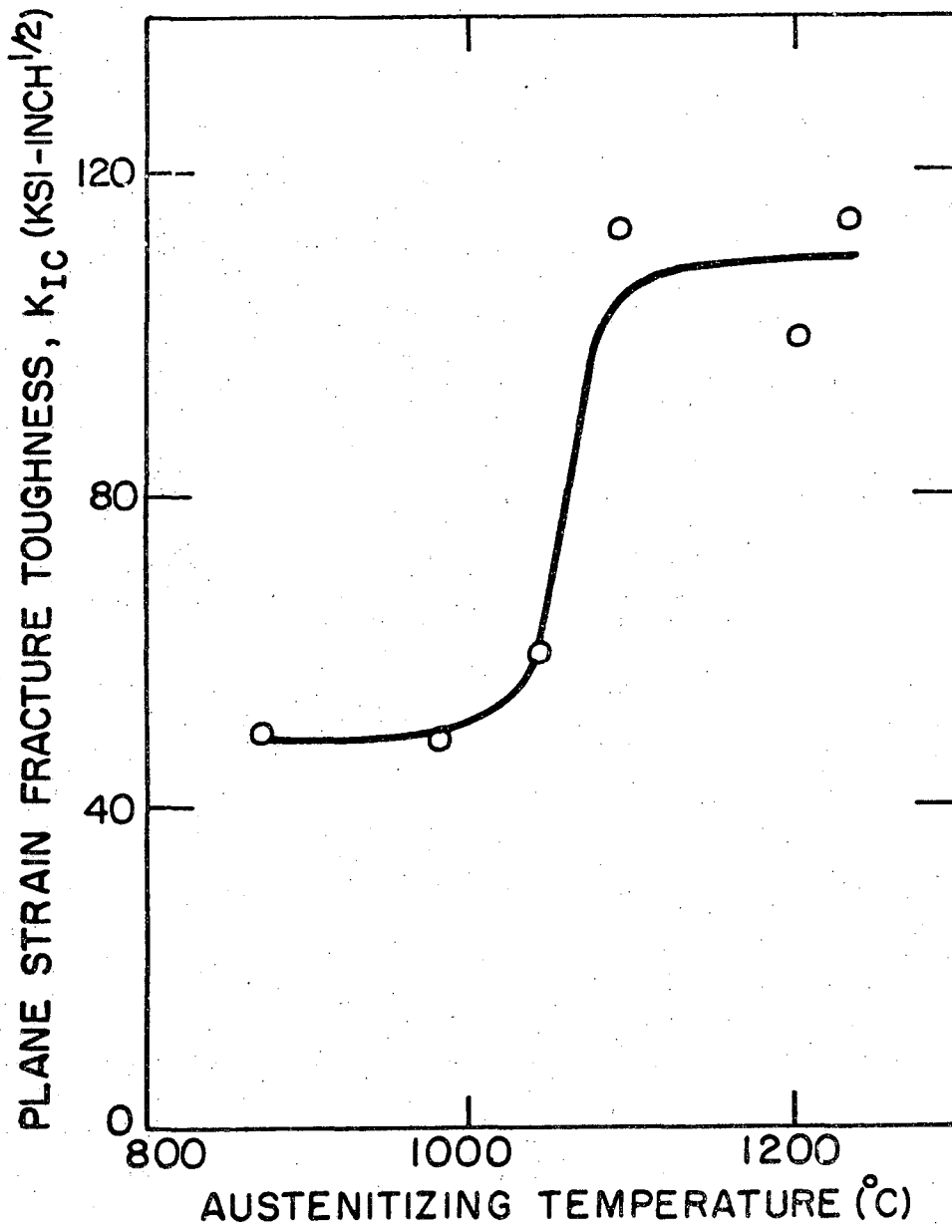
Fig. 19



XBL738-1773

Fig. 20





XBL 733-5913A

Fig. 21



XBB 735-3368

1μ

Fig. 22

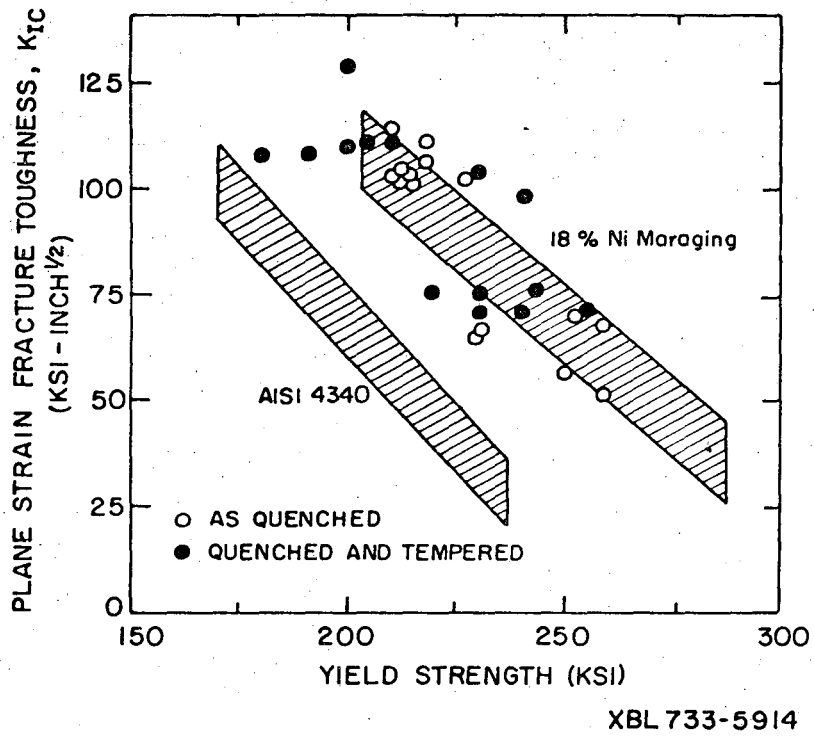


Fig. 23

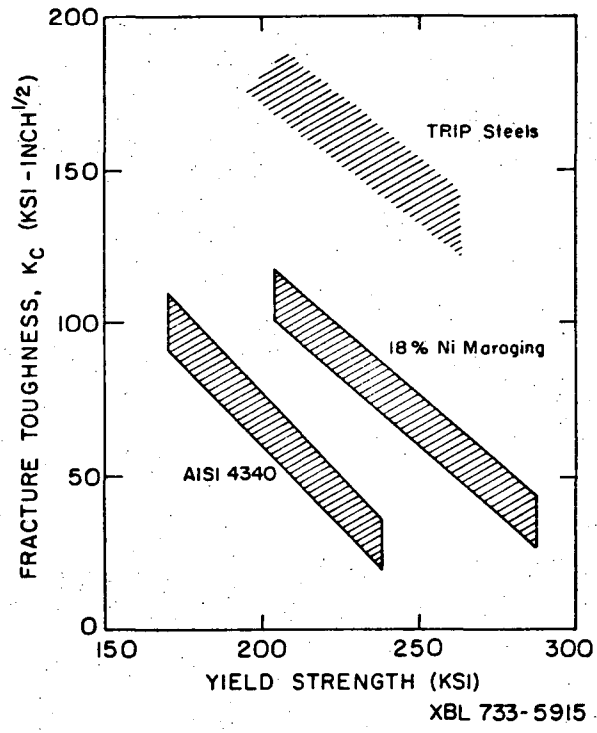


Fig. 24

LEGAL NOTICE

*This report was prepared as an account of work sponsored by the United States Government. Neither the United States nor the United States Atomic Energy Commission, nor any of their employees, nor any of their contractors, subcontractors, or their employees, makes any warranty, express or implied, or assumes any legal liability or responsibility for the accuracy, completeness or usefulness of any information, apparatus, product or process disclosed, or represents that its use would not infringe privately owned rights.*

TECHNICAL INFORMATION DIVISION  
LAWRENCE BERKELEY LABORATORY  
UNIVERSITY OF CALIFORNIA  
BERKELEY, CALIFORNIA 94720